LA-UR-01-3734

TITLE: STRUCTURAL ANALYSIS OF APT SUPERCONDUCTING CAVITIES

AUTHOR(S): Dale L. Schrage LANSCE-1

SUBMITTED TO: Informal Distribution - Internal and External

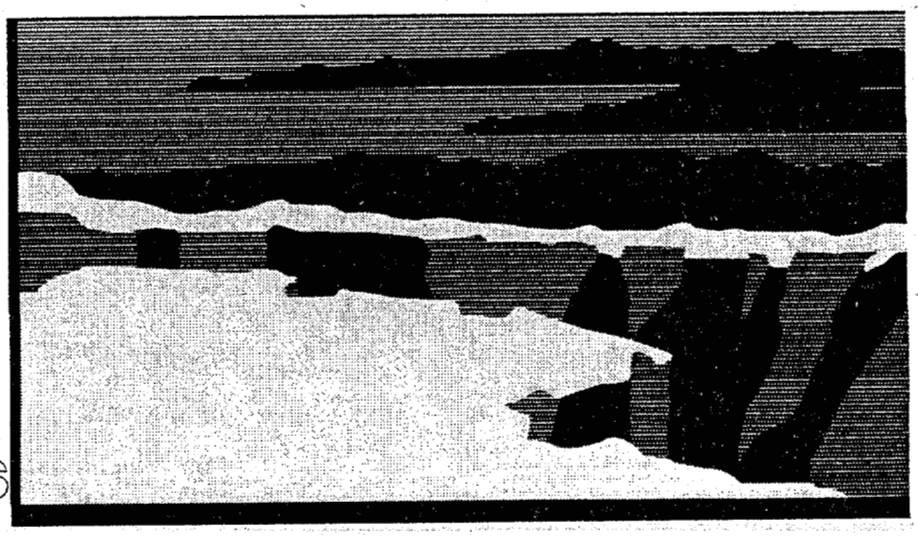

Los Alamos
NATIONAL LABORATORY

Form No. 836 R5
ST 2629 10/91

Los Alamos
NATIONAL LABORATORY

memorandum

Accelerator Operations and Technology Division
Group AOT-1

To/MS: Distribution
From/MS: Dale L. Schrage, MS H817
Erik Swensen, MS H821
Phone/FAX: 7-1953/5-2904
Symbol: AOT-1:95-180
Date: August 28, 1995

SUBJECT: Structural Analysis of APT Superconducting Cavities

Predictions of the static and dynamic structural performance of low-β superconducting elliptical niobium cavities for the APT linac were carried out. It was determined that a stiffened 4-cell 700-MHz cavity at β = 0.428 would have sufficient strength to resist the vacuum load at ambient temperature and would have a minimum resonant frequency of 110 Hz. On the basis of these results, it is concluded that such cavities are structurally adequate for the APT linac starting at 100 MeV.

The original baseline design for the linac for the Accelerator Production of Tritium (APT) is described in reference I-1. Since then (1990) there have been changes in the selected linac structures and the baseline design is presently a normal conducting CW design consisting of a 7-MeV RFQ (ref. I-2), a CCDTL (ref. I-3) to 100 MeV, and a side-coupled linac (ref. I-4) to 1000 MeV.

In January of 1995 is was suggested that considerable reduction in the operating costs of the APT linac could be achieved by replacing the higher energy portion (> 100 MeV) of the linac with a superconducting accelerator. The purpose of this note is to document static and dynamic structural analyses of the low-β elliptical cavities for the superconducting (SC) concept of the APT linac. In addition, the structural performance of elliptical superconducting cavities at lower energies (40-MeV) was also investigated.

I. REQUIREMENTS

The specifications of the APT SC linac are established by the general requirements of the project: beam current, beam halo, beam loss, resonant frequency, initial/final energies, etc. The extent of the beam-halo and beam-loss requirements mainly affect the bore of the cavities. The basic physics specifications are given on Table I-1 on the following page.

TABLE I-1:
APT SC LINAC PHYSICS SPECIFICATIONS

PARAMETER	VALUE
Beam Current	100 mA
Initial Energy	100 MeV
Final Energy	1000 MeV
Resonant Frequency	700 MHz
Bore Radius	5.0 cm @ w<261 MeV 7.5 cm @ w>261 MeV

The cavities selected are nonreentrant elliptical cavities. There are some special requirements that affect the structural design more directly. These and their effects are given in the following table.

TABLE I-2
APT SC LINAC DESIGN REQUIREMENTS & PARAMETERS

REQUIREMENT/PARAMETER	EFFECT
Material: High RRR (~250) Niobium	Yield Strength (σ_y) ~ 7000 #/in^2
No Heat Treatment	Yield Strength (σ_y) ~ 7000 #/in^2 Allows stainless steel flanges & CONFLAT™ or HELICOFLEX™ seals
4 Cells/Cavity	Allows higher structural resonances
Material Thickness: 1/8th inch	Required to avoid quench Minimal effect on stiffness
10 & 15 cm Diameter Bore	Required for high Bore/Beam ratio Establishes minimum iris curvature
Immersion Cooling	No coolant tubes required
Non-immersion chemical polishing	Allows stainless steel flanges & CONFLAT™ or HELICOFLEX™ seals

Niobium with RRR = 250 is readily available both in the US and Europe. Higher RRR base material is also available albeit at higher cost. Similarly, for the peak surface fields planned for the APT-SC-linac heat treatment to improve the RRR is not required. Use of either higher RRR base material and/or heat treatment would increase the cost and produce larger grain size with correspondingly lower yield strength. With the number of cavities required for the APT SC Linac, a total of 464, the cost savings of not requiring higher RRR base material and heat treatment is worthwhile.

The material thickness of 1/8th inch allows fabrication of the half-cells by conventional deep drawing techniques which require that the cavity thickness be less than the forming radius. With chemical polishing only on the interior of the cavity (no immersion) and without a requirement for heat treatment it is possible to utilize CONFLAT™ or HELICOFLEX™ vacuum seals. An alternative would be to use a high strength alloy of niobium such a WC103 for the flanges as was done on the LANL 4-cell cavity (ref. I-5) with HELICOFLEX™ seals. This material costs as much as high RRR niobium and the requirement for the seven flanges would be nearly equal to the volume and cost of the high RRR niobium for the cavities.

The present concept incorporates 4-cell cavities of two types: $\beta = 0.428$ from 100 to 261 MeV and $\beta = 0.710$ (361 MeV) from 261 to 1000 MeV. The use of only two cavity-β values was possible because of the velocity acceptance of the cavities. The $\beta = 0.428$ 4-cell cavity is shown on Figure I-1. It incorporates stiffeners between the half-cells and also between the end half-cell and the end flange. The configuration of four accelerating cells per cavity evolved after study of the existing proven waveguide windows. This was convenient with regard to keeping the structural resonances above 60 Hz. This is discussed in detail in Section VI.

II. MATERIALS

The thermal regime of interest is at ambient temperature. High purity niobium (RRR ~250) has very high strength (σ_y & σ_u > 100,000 #/in^2) at cryogenic temperatures (ref. II-1). At ambient temperatures, the yield strength drops more than an order of magnitude. Thus, the worst static load case is vacuum loading of the cavity while at ambient temperature. For the purpose of the structural analyses, the properties in Table II-1 were used.

TABLE II-1:
PROPERTIES OF NIOBIUM AT AMBIENT TEMPERATURE

PROPERTY	metric Units	English Units
Density ρ	8.66 gm/cm^3	0.31 #/in^3
Modulus E	0.99 GPa	1.43 X 10^7 #/in^2
Yield Strength σ_y (0.5%)	103 MPa	7,000 #/in^2
Poisson's Ratio ν	0.38	0.38
Thermal Exp Coeff α	7.6 X 10^{-6} /°C	4.2 X 10^{-6} /°F

Thin sections of high RRR niobium exhibit stress-strain behavior similar to that of annealed OFE copper except that work-hardening does not occur. A proportional limit and the yield strength are not well defined. As in the case of copper, the yield strength

is defined at 0.5 per-cent offset. For the sake of these analyses it has been assumed that a limited amount of local yielding will be permitted, mostly in areas of stress concentration near the weld joints. As a design criteria, the von Mises stress should not exceed 5000 #/in^2 over most of the cavity.

III. CELL GEOMETRY

The cell geometries selected are nonreentrant "elliptical" shapes. These have been reliably produced by a deep drawing and welding process at many laboratories and in industry. The non-re-entrant shape assures that the cavities will drain chemicals and water reliably. The present concept of the APT SC linac incorporates but two different cell geometries, $\beta = 0.428$ (w = 100 MeV) and $\beta = 0.710$ (w = 361 MeV). At the higher energies, the rms beam size increases so a larger bore, 7.5-cm radius versus 5.0-cm radius, is required. As the physics design is refined, it may be necessary to incorporate a larger number of cavity shapes or different shapes than those discussed herein.

The analysis concentrated on the worst case, 100 MeV ($\beta = 0.428$). Figure III-1 shows a comparison of four cavity shapes at 700 MHz, $\beta = 0.283$ (40 MeV), $\beta = 0.428$ (100 MeV), $\beta = 0.710$ (361 MeV), and $\beta = 1.0$. The $\beta = 0.283$ and $\beta = 1.0$ cross-sections are shown for comparison. The inability of an un-stiffened $\beta = 0.428$ cavity to support a vacuum load is obvious. The detailed geometry of the $\beta = 0.428$ (100 MeV) half-cell is shown on Figure III-2. Note that for the purpose of structural analysis, the elliptical segment at the iris has been replaced with two shorter circular sections of comparable curvature. The structural analysis codes do not support elliptical shapes. Until recently, SUPERFISH did not support elliptical shapes either.

For the sake of completeness, some analysis of a $\beta = 0.710$ (361 MeV) cavity was also carried out. Its geometry is shown on Figure III-3. As the energy is increased, the rigidity of the half-cell and the 4-cell cavity is improved so detailed structural analysis is not warranted at this early conceptual design stage.

There was also a question regarding the lowest energy at which the elliptical cavities could be utilized without going to unreasonable efforts. A 40-MeV ($\beta = 0.283$) single cell cavity was also analyzed as part of the consideration for extending the energy where the superconducting linac begins. Its geometry is shown on Figure III-4. The $\beta = 1.0$ geometry is shown on Figure III-5 for completeness.

IV. SINGLE CELL STATIC ANALYSIS

Analyses of 100-MeV ($\beta = 0.428$) single half-cells were carried out to determine stiffness, stress levels, tuning forces, and locations for stiffeners. This is the worst case; higher β

cavities will be stiffer. For most of these analyses, a material thickness of 0.110 inch was used to compensate for the material removed in the chemical polishing process. The geometry for this cavity is shown on Figure III-2. A limited amount of analysis of the β = 0.710 (361 MeV) cavity shown on Figure III-3 was also carried out. As a matter of academic interest, two models were generated for a 40-MeV (β = 0.283) cavity. The models used are listed in Table IV-1.

TABLE IV-1:
APT-SUPERCONDUCTING-HALF-CELL-ANALYSIS MODELS

MODEL	ENERGY MeV	Beta β	THICK. inch	WELD JOINT	DESCRIPTION
APTSCA1	100	0.428	0.125	yes	ORIGINAL (ellipsoidal)
HALFPLAT	100	0.428	0.125	no	ORIGINAL (ellipsoidal)
APTSCA2	100	0.428	0.110	yes	REVISED (toroidal)
APTSCB1	40	0.283	0.110	yes	ORIGINAL (toroidal)
APTSCC1	40	0.283	0.110	yes	APTSCB1 with 0.38 in thick Cu
APTSCD1	361	0.710	0.110	yes	ORIGINAL (toroidal)
APTSCE1	>1000	1.000	0.110	yes	ORIGINAL (toroidal)
CERN1	>1000	1.000	0.235	no	Toroidal

The structural analysis was carried out using COSMOS/M® version 1.71. Axisymmetric PLANE2D elements were used with the material properties as given in Table II-1. Only linear static analyses were performed. The first model, APTSCA1, has a weld joint and uses a material thickness of 0.125 inch. The weld joint is modeled as a reduction in thickness to 0.063 inch at the iris and equator. The second model, HALFPLAT, was created using the same geometry but without the weld joint. This model, with the material thickness reduced to 0.110 inch to account for the chemical polishing, was used to generate the three-dimensional models used for the static and dynamic analyses of the multi-cell cavities. These two models were created using MAFIA and originally had ellipsoidal shapes. The third model, APTSCA2, had slightly revised geometry which utilized toroidal shapes created from SUPERFISH. Most of the work was done with the third model. Two 40-MeV models, a β = 1 model, and the 350-MHz CERN-LEP (β = 1) half-cell were also analyzed. The results of the analyses are given on Table IV-2 on the following page.

For the models with the iris not constrained, it was assumed that there would be a bellows in the beam line and therefore the vacuum load on the beam pipe was not included. All of the analyses used a symmetric boundary condition at the equator.

TABLE IV-2:
APT SUPERCONDUCTING HALF-CELL ANALYSIS RESULTS

MODEL #	RUN #	BOUND COND @IRIS	STIFF RADIUS inch	PRESS. #/in²	IRIS FORCE #	STIFF FORCE #	MAX AXIAL DEFLECT inch	MAX von Mises STRESS #/in²	FREQ. SHIFT Hz	NOTES
APTSCA1	01	Free	None	Amb.	N/A	N/A	-0.060028	15057	——	
APTSCA1	02	Fixed	None	Amb.	986	N/A	-0.008808	13584	——	
HALFPLAT	01	Fixed	None	Amb.	N/A	N/A	-0.008150	6078		
APTSCA2	01	Free	None	N/A	N/A	N/A	0.000758	N/A	$-2.78\ 10^5$	0
APTSCA2	02	Free	None	Amb.	N/A	N/A	-0.061875	16070	$-7.45\ 10^6$	
APTSCA2	03	Free	None	0	100	N/A	-0.007760	2202	$-9.97\ 10^5$	1
APTSCA2	04	Fixed	None	Amb.	782	N/A	-0.011600	13592	$1.20\ 10^5$	
APTSCA2	05	Fixed	4.58	Amb.	293	1042	-0.001050	3984	$2.27\ 10^4$	
APTSCA2	06	Fixed	4.58	0	-2	-48	-0.001060	879	$-1.07\ 10^5$	3
APTSCA2	07	Fixed	4.58	Amb.	290	957	-0.001890	4079	$-8.40\ 10^4$	3
APTSCA2	08	Fixed	4.00	Amb.	177	999	-0.002280	5602	$1.83\ 10^5$	
APTSCA2	09	Fixed	4.66	Amb.	316	1057	-0.001000	4349	$-8.52\ 10^3$	2
APTSCA2	10	Fixed	4.58	Amb.	276	990	-0.001740	4079	$-8.74\ 10^4$	4
APTSCB1	01	Free	None	Amb.	N/A	N/A	-0.162000	62424	$-3.10\ 10^7$	
APTSCB1	02	Fixed	None	Amb.	1039	N/A	-0.022200	22994	$1.62\ 10^6$	
APTSCB1	03	Fixed	4.98	Amb.	393	1311	-0.001500	5196	$9.34\ 10^4$	
APTSCC1	01	Free	None	Amb	N/A	N/A	-0.013400	6822	$-2.84\ 10^6$	
APTSCC1	02	Fixed	None	Amb.	183	N/A	-0.000653	4538	$4.32\ 10^4$	
APTSCD1	01	Free	None	Amb	N/A	N/A	-0.016674	7818	$-1.28\ 10^6$	
APTSCD1	02	Fixed	None	Amb.	748	N/A	-0.003032	5491	$5.98\ 10^3$	
APTSCD1	03	Fixed	5.03	Amb.	304	937	-0.000412	2307	$-2.96\ 10^3$	
APTSCD1	04	Fixed	5.03	0.	-21	233	-0.001075	1465	$-5.46\ 10^4$	3
APTSCE1	01	Free	None	Amb	N/A	N/A	-0.003972	3832	$-2.00\ 10^6$	
APTSCE1	02	Fixed	None	Amb.	429	N/A	-0.001170	3580	$-1.11\ 10^4$	
APTSCE1	03	Fixed	4.45	Amb.	99	562	-0.000156	1532	$9.13\ 10^3$	
CERN1	03	Fixed	N/A	0.	220	N/A	-0.00100	443	$-1.20\ 10^4$	3

Notes:
0 Uniform Temp Increase of 100 °F
1 100# Force Applied @ Iris
2 Frequency Shift Due Ambient Pressure Nulled
3 -0.001 inch Displacement @ Iris & Stiffener
4 -0.001 inch Displacement @ Iris, -0.00064 inch Displacement @ Stiffener

$\beta = 0.428$ HALF-CELL:

Model APTSCA1/Run 01 was for the cavity not constrained at the iris and under atmospheric pressure (vacuum load). The maximum stress, 15057 #/in², is far beyond the yield stress and stresses in excess of 10000 #/in² occur over a large portion of the cavity. This would lead to collapse of the cavity. This would have been evident had a analysis of the cavity been run which incorporated geometric non-linearities plus the effect of yielding. Therefore, it is clear that the iris must be constrained (fixed) if the

cavity is to support a vacuum load at ambient pressure. This places a requirement for special care to be taken during vacuum leak checking of un-stiffened 100-MeV structures.

Model APTSCA1/Run 02 was for the case of the cavity constrained at the iris. While the maximum von Mises stress is not reduced significantly, the maximum occurs in the weld area. Over most of the cavity wall, the stress does not exceed 5000 #/in^2. This cavity will not collapse but has inadequate stiffness. A 4- or 6-cell cavity would have unacceptably high bending deformations (see Section V) and unacceptably low structural resonant frequencies (see Section VI).

Model HALFPLAT was created to check the effect of the reduced thickness at the weld joint. The results of model HALFPLAT/Run 01 show that effect of the weld joint upon the maximum displacement is small (0.0088 inch with the weld joint verses 0.0082 inch without the weld joint). This model was also used to generate the geometry for the analyses of the multi-cell cavities.

For models APTSCA2 and HALFPLAT, the elliptical cross-sections modeled in MAFIA were replaced with approximate circular arcs. Subsequent analyses utilized cavity cross-sections from SUPERFISH. These cross-sections were made up of circular arcs and straight lines. Use of SUPERFISH allowed the frequency shifts to be determined directly.

Most of the analysis cases were run on model APTSCA2. This model has weld joints and uses a material thickness of 0.110 inch. Run 01 was carried out to test the validity of the frequency-shift analysis. The results should be a frequency shift given by

$$\delta F = - \alpha \, \delta T \, F$$

For the 700-MHz niobium cavity with a 100°F temperature rise, the frequency shift should be -2.94 X 10^5 Hz which is only five per-cent higher than the value calculated by the combination of SUPERFISH, COSMOS/M, and the AOT-1 code SHIFTFRQ. This is satisfactory accuracy.

Model APTSCA2/Run 02 is a comparison to Model APTSCA1/Run 01 to see the effect of the smaller material thickness and to see the differences between the ellipsoidal and toroidal shapes. These differences are small. With the iris un-constrained, this cavity would collapse under vacuum load. This would have been evident had a non-linear analysis of the cavity been run. The axial displacements for this case are shown on Figure IV-1. The displacements are amplified by a factor of 5.

Model APTSCA2/Run 04 and APTSCA1/Run 02 are comparable for the case where the iris is constrained. This comparison shows the effect of the reduced thickness. The axial displacements for model APTSCA2/Run 04 are shown on Figure IV-2. The displacements are amplified by a factor of 25.

It is clear that even with the iris constrained, the displacements, stresses, and resonant frequency shifts of the cavity are unacceptably large. Some additional stiffening is therefore required. As a first step, a cylindrical stiffener was added at the radius where the iris-constrained cavity had the maximum displacement, 4.58 inches. As far as fabrication, each stiffener would be a 1/8th inch thick split ring with through holes to allow the cryogen to pass. The stiffeners would be made of high purity (but not RRR grade) niobium and would be attached as the final welding step. There are also stiffeners which connect the end half-cells to the beam tubes. This stiffener concept is very similar to that proposed for the TESLA cavities (ref. IV-1). The exploded 4-cell cavity is shown on Figure VI-3.

The stiffened cavity was analyzed as model APTSCA2/Run 05. The stiffener was modeled as an axial constraint of the outer nodes nearest to the radius of 4.58 inches. The axial displacements are shown on Figure IV-4. The displacements are amplified by a factor of 200. The presence of the stiffener reduced the maximum displacement by a factor of 10, the maximum stress by a factor of four, and the frequency shift by a factor of five. Clearly the addition of the stiffener is worthwhile. Its value is further demonstrated in the discussions which cover the static and dynamic analysis of the multi-cell cavities.

Model APTSCA2/Runs 06 and 07 were made to determine the tuning sensitivity. From Run 06, the tuning sensitivity is -1.07×10^5 MHz per 0.001 inch inward displacement of the half-cell iris. For the complete 4-cell cavity, the tuning sensitivity is -13 KHz/0.001 inch (527 MHz/micron). This scales with frequency, the ratio of the equator/iris radii, and energy (β) from the values reported in reference IV-2.

Model APTSCA2/Runs 08 and 09 were made to determine the sensitivity to the radius of locating the stiffener and to find a radius where the frequency shift due to the vacuum load was nulled. These results may be compared with Run 05. The conclusion is that the frequency shift due to the vacuum load is quite sensitive to the position of the stiffeners. The cavities will have active tuners so this is not a problem.

Model APTSCA2/Run 10 takes into account that the stiffener has finite stiffness. This should be compared to model APTSCA2/Run 07. The differences are small.

β = 0.710 HALF-CELL:

A 361 MeV (β = 0.710) half-cell (model APTSCD1) was also analyzed. The geometry for this half-cell is shown on Figure III-3. The results of model APTSCD1/Run 03 (Figure IV-5) may be compared to those of model APTSCA2/Run 05. The maximum stress and displacement of the β = 0.710 half-cell under a vacuum load are significantly lower than those of the β = 0.428 half-cell. Therefore it was concluded that the results of the analysis of the β = 0.428 half-cell would be sufficient to verify that the stiffness of the β = 0.710

was adequate. With limited personnel resources and time, further analyses of the β = 0.710 cavity was not warranted. The tuning sensitivity of this cavity is 378 Hz/micron.

β = 0.283 HALF-CELL:

Two versions of a 40-MeV (β = 0.283) half-cell were analyzed as part of the consideration of lowering the energy at which the superconducting linac is utilized. The geometry for this half-cell is shown on Figure III-4. The first run, model APTSCB1/Run 01, was made without the iris constrained and showed that the cavity would collapse. With the iris constrained, model APTSCB1/Run 02, the stresses, at 22944 #/in^2, are excessive. With the addition of a stiffener, model APTSCB1/Run 03, the cavity becomes closer to the behavior of the β = 0.428 cavity. The displacements are shown on Figure IV-6.

COPPER-PLATED HALF-CELL:

An alternative to use of welded-on stiffeners would be to add a thick layer of high thermal conductivity high strength copper by electroplating (ref. IV-3. The electroformed copper has a yield strength in excess of 28000 #/in^2 at ambient temperature. Two runs on the 40-MeV (β = 0.283) copper-plated half-cell were carried out. This half-cell had a 0.375 inch thick layer of copper-plated onto the niobium. For a cavity without the iris constrained, model APTSCC1/Run 01, the stresses (6822 #/in^2 maximum) were quite close to the acceptable level (5000 #/in^2). With the iris constrained, APTSCC1/Run 02, the performance of the cavity was satisfactory. The displacements are shown on Figure IV-7. While this appears to be an elegant solution for single or multi-cell cavity, the electroplating process becomes less straight-forward when the complications of the rf power and higher-order-mode couplers are added.

Our conclusion from the analysis of the 40-MeV (β = 0.283) half-cells was that extension of the elliptical cavities much below 100 MeV (β = 0.428) would be difficult from the point of view of the structural performance and would require careful modeling as well as some hardware experiments before this should be considered a dependable solution.

β = 1 HALF-CELL:

For comparison, a β = 1 cavity (Figure III-5) was also analyzed. The results (model APTSCE1) show that this cavity, even without constrained ends, would adequately support the vacuum load.

CERN LEP HALF-CELL:

In order to benchmark the half-cell analysis, a model of the CERN LEP interior half-cell (ref. IV-4 was analyzed. The analysis (model CERN1/Run 03) predicted a frequency sensitivity of 45 Hz/micron. The reported value for the CERN 4-cell LEP cavity is 40 Hz/micron (ref. IV-2). The small difference is attributed to the effects of the ends cells, which are different, and the presence of the beam tubes, rf coupler, and HOM coupler.

V. MULTI-CELL STATIC ANALYSIS

Early designs of the 700-MHz superconducting rf cavity called for two 6-cell cavities to be placed in each cryostat. This led to the static analysis of both the 6-cell and 12-cell rf cavities. Further refinement of the physics design resulted in the use of a 4-cell cavity. A static analysis using finite-element methods was performed to examine both the bending and axial deformations of each cavity design. Gravitational loads in the transverse and axial directions were examined as well as the deformations that will result when the cavity is operated under extreme vacuum. The results of this analysis are given in the following pages.

Model Development:

Two-dimensional axisymmetric models were used to develop element meshes, to verify cavity shapes, and to select the arrangements of stiffeners. This is described in Section IV. The axisymmetric model HALFPLAT was used to generate the three-dimensional models. Figure V-1 shows the full model of the 6-cell cavity used to calculated the transverse and axial deformations. Again, the model was able to take advantage of symmetry and model only half the cavity along the axial plane. Anti-symmetric loads limited the amount of model reduction that could be exploited. Figure V-2 shows the finite-element model of the 4-cell cavity used in the static analysis. An accurate full 12-cell model exceeds the upper-element-limit capability of the finite-element code, therefore the right end of the 6-cell cavity was constrained with symmetric boundary conditions to model the 12-cell cavity. Symmetric boundary conditions constrain axial deformations that result from the axial gravitational load. They are not considered herein. Post-analysis physics-design changes eliminated the 12-cell design from further study, however the results will be tabulated as a reference.

The element type and mesh density were studied to determine the best parameters that would produce the greatest accuracy. In-plane and out-of-plane deformations made the element selection difficult. Plane stress elements were not considered because of the out-of-plane loads. Quadrilateral shell elements produced errors as large as 24%. There is an apparent flaw in the way COSMOS/M® (Version 1.71) formulates the quadrilateral shell element that may cause the results to be off by as much as 200% for in-plane bending loads. These errors can be reduced by increasing the mesh density. Triangular shell elements give better results for in-plane and out-of-plane bending, thereby providing the best results.

The mesh density was changed to determine the largest element size that would give good results relative to the axisymmetric model. Four element sizes were considered: 0.9, 0.6, 0.4, and 0.3. Table V-1 gives the results of this trade study. Clearly an element size of 0.3 will give the best results.

TABLE V-1:
COMPARISON OF FULL MODEL DEFORMATIONS RELATIVE TO THE AXISYMMETRIC BASELINE MODEL

Element Size	Max. Pressure Deformation (in)	% Error
Baseline	0.00820	0.00%
0.9	0.00710	13.41%
0.6	0.00780	4.88%
0.4	0.00821	-0.12%
0.3	0.00820	0.00%

*Note: These deformations are based on a wall thickness of 0.125". The thickness used in the multi-cell analysis was 0.110".

Static Analysis of the Un-Stiffened Cavities:

The purpose of the analysis was to investigate the static response of each cavity design. The cavity had to resist both bending and axial deformations that result from gravitational loads in the transverse and axial directions as well as a pressure load of one atmosphere applied to the outer shell. The bending deformations of the 4-, 6-, and 12- cell cavities are large enough to distort the beam line and would require constraints to reduce the total deformation. As expected, the stiffness is significantly improved from the 12-cell to the 6-cell and again from the 6-cell to the 4-cell cavity due to the differences in length of the three cavities. Figure V-3 shows the transverse deformations that result from applying a gravitational load in the transverse direction. Table V-2 summarizes the results of the static analysis of the multi-cell cavities.

TABLE V-2:
DEFORMATIONS OF MULTI-CELL CAVITIES

Cavity Model	Maximum Deflection (inch)		
	Transverse Gravitational	Axial Gravitational	Ambient Pressure
4-Cell	0.00318	0.00377	0.01220
6-Cell	0.01250	0.00850	0.01240
12-Cell	0.17000	N/A	0.01240

An axial response in the cavity is produced by both the gravitational load in the axial direction and the ambient pressure applied to the outer surface of the cavity. The axial

deformations for the 4-cell cavity that result for each load case are shown in Figures V-4 and V-5 respectively.

Figure V-5 shows the deformations that result from an ambient pressure applied to the outer cavity surface. These results are also listed in Table V-2. The axial deformations become important because they cause a shift in the cavity frequency. The deformations that result from the gravitational load in the axial direction are less desirable than those produced by the ambient pressure because the frequency shift will be different from cell to cell. While this is not a problem for the in-service cavities which will be mounted in a horizontal orientation, this would affect tests of the cavities in a vertical cryostat. The symmetry of the ambient-pressure deformations for each half-cell gives an equivalent frequency shift in each cell. This will be easier to control than the gravitational deformations.

The axial deformations that result from a transverse gravitational load are proportional to the transverse displacements and will require some constraint. The 12-cell cavity was not considered in this portion of the analysis because the size of the model exceeded the limitations of the PC-version of COSMOS/M®. The ambient-pressure deformations listed in Table V-2 are not dependent on the number of cells or the length. The symmetric geometry and loading drive the results of the full cavity models to match those of the half-cell model. Note the results given in Table V-1 are based on a wall thickness of 0.125 inch while those given in Table V-2 are based on a wall thickness of 0.110 inch.

Static Analysis of Stiffened Cavities:
The axial deformations that occur from the ambient pressure are greater than desired, therefore, several stiffener concepts were considered to reduce these deflections. The selected concept is shown on Figure I-1 with an exploded view on Figure IV-3. Figure V-6 shows the finite-element model of the 4-cell cavity with stiffeners. The model is simplified in that the rf couplers, rf probes, and higher order mode couplers are not included. Cylindrical stiffeners were used between each cell and conical stiffeners were used on each end half-cell. The conical stiffeners were optimized to provide a stiffness to the outer half-cell that is equivalent to the stiffness of the inner half-cells provided by the cylindrical stiffeners. This is necessary to assure an equivalent wall displacement of each half-cell so that field flatness is maintained when the cavity is tuned.

The results are listed in Table V-3 on the following page. The results show that the deformations under all loading cases are significantly reduced from those of the un-stiffened cavities. The large reduction in the deformation due to the ambient-pressure load is accompanied by a similar reduction in the stress.

TABLE V-3:
SUMMARY OF DISPLACEMENT RESULTS WITH STIFFENERS

Cavity Model	Maximum Un-stiffened Deformation inch	Maximum Stiffened Deformation inch	% Change
Transverse Gravitational Load			
4-Cell	0.00318	0.00054	-83%
6-Cell	0.01250	0.00077	-94%
Axial Gravitational Load			
4-Cell	0.00377	0.00113	-70%
6-Cell	0.00850	0.00135	-84%
Ambient Pressure Load			
4-Cell	0.01220	0.00130	-89%
6-Cell	0.01240	0.00127	-90%

Static Analysis of Copper Plated Cavities:
A second method of stiffening the cavity is to plate the cavity with a 1/2-inch-thick layer of copper. Copper is selected because of its high thermal conductivity. The heat from the rf load will easily conduct through the cavity walls, this will avoid quenching of the superconducting cavity.

The copper-plated cavity has both advantages and disadvantages over the stiffened cavities. On the positive side, the axial stiffness, as well as the transverse stiffness, is increased substantially. The weight, however, is increased substantially as well. The model used in this analysis is the same as the un-stiffened model, but uses a laminate-shell element to represent the copper and niobium layers. Both transverse and axial displacements are improved relative to the stiffened cavity and the deflections that result from an ambient-pressure load are reduced by more than 90%. These results are summarized in Table V-4 and can be compared to the results of the stiffened cavity in Table V-3.

The maximum deformations of the copper-plated cavities are smaller than those of the stiffened cavities for each load case with the exception of the transverse gravitational load on the 6-cell cavity. The deformation due to the axial gravitational load is improved by a factor of two and the deformation due to the ambient pressure load is reduced by nearly an order of magnitude relative to the stiffened cavities. These improvements do not come without a penalty. The additional material will drive the weight of the structure up by nearly a factor of four.

TABLE V-4:
SUMMARY OF DISPLACEMENT RESULTS WITH COPPER PLATING

Cavity Model	Maximum Un-stiffened Deformation inch	Maximum Plated Deformation inch	% Change
Transverse Gravitational Load			
4-Cell	0.00318	0.00045	-21.1%
6-Cell	0.01250	0.00126	103.2%
Axial Gravitational Load			
4-Cell	0.00377	0.00045	-57.1%
6-Cell	0.00850	0.00099	-17.5%
Ambient Pressure Load			
4-Cell	0.01220	0.00018	-98.3%
6-Cell	0.01240	0.00019	-98.3%

VI. MULTI-CELL DYNAMIC ANALYSIS

There is one inherent problem that will occur during operation of the accelerator: the cavities will be exposed to ambient noise sources. Ambient noise sources have an undesirable impact on the particle beam because they have large amplitudes at low frequencies (<~120 Hz). These large displacements in the cavity can lead to growth of the accelerated-beam transverse and longitudinal phase space. The natural frequencies of the cavity can be increased by stiffening the cavity. The result would de-couple the natural frequencies of the cavity from the large amplitude lower frequency ambient noise sources.

A modal survey of the APT superconducting rf cavity designs was completed using finite-element techniques. COSMOS/M® finite-element code was used to build three-dimensional models of the 12-cell, 6-cell, and 4-cell cavities. The first ten modes were examined to determine the natural-frequency crossover within the low frequency bandwidth. The following describes the results found in this modal survey.

Dynamic Analysis of Un-Stiffened Cavities:
The initial analysis was performed on un-stiffened 6-cell and 12-cell cavities. Figure VI-1 shows the finite-element model of the 6-cell cavity design. This and the other models used for the dynamic analysis were simplified in that the rf couplers, rf probes, and HOM couplers are not included. Their presence would serve to reduce the resonant

frequencies and produce coupling between the transverse and axial modes. At the time of final design it will be necessary to analyze the complete unsimplified structure.

The 12-cell cavity was simply two 6-cell cavities placed in line inside the cryostat. Early designs allowed for motion in the axial and transverse directions of the center beam tube. Figure VI-2 shows the finite-element model of the 12-cell cavity. This model could not take advantage of symmetry because the center constraints would constrain axial modes with odd mode shapes and force all of the mode shapes found by the model to be even. Odd mode shapes can be described as those modes with motion depicted by $n\pi$, assuming axial harmonic motion, for odd values of n (i.e., n = 1, 3, 5, ...). Even mode shapes, as expected, have even values of n. The results will thereby give misleading frequency results. The boundary conditions are fixed-fixed for each of the finite-element models in this dynamic analysis.

Later modifications to the design resulted in a 4-cell cavity. The elliptical shape of each cell was left unchanged for purposes of this analysis and the boundary conditions remained the same, fixed-fixed. Figure VI-3 shows the finite-element model of the 4-cell cavity.

The results obtained from this analysis showed that the cavities natural frequencies were unacceptably low. Table VI-1 lists the first three transverse and first two axial modes found. Each transverse mode has an orthogonal counterpart, one in each of the two transverse coordinate planes. As shown, the first transverse mode of the 12-cell cavity is 8.6 Hz. This is clearly too low and will resonate with larger amplitudes from the ambient noise sources. This frequency can be increased to 30.8 Hz by constraining the center in all directions (this is also accomplished with a 6-cell cavity design).

TABLE VI-1:
NATURAL FREQUENCIES OF THE UN-STIFFENED CAVITIES

Mode	Frequency (Hz)		
	12-Cell	6-Cell	4-Cell
1st Transverse	8.6	30.8	57.0
2nd Transverse	15.6	60.7	92.4
3rd Transverse	36.2	86.6	111.8
1st Axial	19.0	39.4	60.2
2nd Axial	39.4	78.5	118.7

The first transverse mode of the 6-cell cavity is 30.8 Hz and the 4-cell cavity is 57.0 Hz. Figure VI-4 shows the deformations of the first transverse mode of the 4-cell cavity. The two beam tubes on the outer ends are significantly stiffer than the cavity region,

therefore, they do not have a critical impact on the stiffness or natural frequency of the cavity.

The axial modes are slightly higher than the transverse modes for each cavity. The first axial modes are 19.0, 39.4, and 60.2 Hz for the 12-cell, 6-cell, and 4-cell cavities, respectively. There is a factor of 2 improvement between the 12-cell and 6-cell cavity stiffness and a factor of 1.5 increase between the 6-cell and 4-cell cavities. Figure VI-5 shows the deformations of the first axial mode of the 4-cell cavity. Again, the stiffness of the beam tubes are much higher than that of the cells, therefore, the natural frequency of the cavity is not affected by the stiffness of the end cylinders.

The modal survey has revealed that the stiffnesses of these cavities are too low. Two solutions were considered and examined that would increase the natural frequency of the cavities. The first considered adding radial and cylindrical stiffeners to each cavity. The stiffness would be increased without increasing the weight significantly. The second solution considered the effect of adding a layer of copper to the niobium cavity. This would increase the stiffness of the cavity with an additional penalty of increasing the weight. Both solutions are considered and evaluated in the following paragraphs.

Dynamic Analysis of Stiffened Cavities:
Radial and cylindrical stiffeners were added to each cavity to increase the natural frequency of the cavities. Figure VI-6 illustrates the stiffeners used on the 4-cell cavity. Cylindrical stiffeners were used to support the iris of each inner cell and conical stiffeners were used to support the iris of each end half-cell. The length and thickness of the conical stiffeners were optimized to provide a stiffness to the outer half-cell that is nearly equivalent to the stiffness of the inner half-cells provided by the radial stiffeners. This is necessary to assure an equivalent frequency shift in each cell when tuning the cavity. The stiffness of the equator is not increased by these stiffeners.

Table VI-2 summarizes the results of the dynamic analysis performed on the stiffened cavities. The natural frequencies of the cavities have increased significantly. The first transverse modes are 19.3 Hz, 66.7 Hz, and 140.7 Hz for the 12-cell, 6-cell, and 4-cell cavities respectively. This is an average increase of 130%, 120%, and 160% for each of the respective cavities in the transverse direction. The axial stiffness was not increased as substantially. The average increase for all three cavities was 80%. The first axial modes are 34.6 Hz, 70.2 Hz, and 109.8 Hz for the 12-cell, 6-cell, and 4-cell cavities respectively. It is clear that the radial and cylindrical stiffeners used to stiffen each cavity provide greater stiffness in the transverse direction than they do in the axial direction. This may become a more significant issue if the ambient noise-source requires the stiffness of the cavity to be greater than currently designed. More material will be required to constrain the axial modes, which in turn, will drive the weight up and natural frequency down. Axial stiffness considerations would have to be examined more closely.

TABLE VI-2:
SUMMARY OF THE MODAL SURVEY WITH STIFFENERS

Mode	Frequency (Hz)		
	12-Cell	6-Cell	4-Cell
1st Transverse	19.3	66.7	140.7
2nd Transverse	36.5	139.9	239.8
3rd Transverse	82.6	212.8	320.7
1st Axial	34.6	70.2	109.8
2nd Axial	70.2	139.8	216.0

Dynamic Analysis of Copper-Plated Cavities:
A second approach to stiffening each cavity was to use a 1/2 inch of copper plating over the entire niobium cavity. The copper plating will provide significant axial as well as transverse stiffness to the cavity and maintain good thermal conductivity. This is crucial for the 4-cell cavity in which the axial stiffness was not increased as substantially as the transverse stiffness resulting in the axial mode becoming the first natural frequency of the cavity. The model used in this analysis was the same as that of the un-stiffened cavity with the exception of some changes to the element type, material properties, and real constants that were modified to include the copper layer.

The results of this analysis are summarized in table VI-3. The 12-cell cavity was not examined in this portion of the modal survey. It is clear by the results shown for the 6-cell and 4-cell cavities that there is a substantial gain in stiffness with the copper plating versus using radial and cylindrical stiffeners. The transverse stiffness has increased on the average by approximately 170% - 200% which is comparable to the increase gained by using the stiffeners previously described. The advantage comes from an average increase of 180% to the axial stiffness versus 80% with the added stiffeners. A torsional mode has become more dominant and resonates at 203.9 Hz and 205.2 Hz for the 6-cell and 4-cell cavities, respectively. Copper plating proves to be a satisfactory means of stiffening the cavity assuming that the displacements that result from the additional weight are acceptable and other issues such as thermal conductivity provide adequate performance. Further refinement of the linac requirements would distinguish the most optimum means of stiffening the cavity.

TABLE VI-3:
SUMMARY OF THE MODAL SURVEY OF THE COPPER-PLATED CAVITIES

Mode	Frequency (Hz)	
	6-Cell	4-Cell
1st Transverse	91.5	149.4
2nd Transverse	181.1	262.7
3rd Transverse	266.9	365.7
1st Axial	110.2	169.3
2nd Axial	221.3	342.1

VII. CONCLUSIONS

40-MeV (β = 0.283) Elliptical Cavities:
The conclusion from the analysis of the 40-MeV (β = 0.283) half-cells was that extension of the elliptical cavities much below 100 MeV (β = 0.428) would be difficult from the point of view of the structural performance and would require careful modeling as well as some hardware experiments before this should be depended upon.

100-MeV (β = 0.428) Elliptical Cavities:
The conclusion from the analysis of the 100-MeV (β = 0.428) is that the stiffened cavity will have adequate stiffness to resist the vacuum load and will have acceptably high structural resonant frequencies (>100 Hz). At the present time, use of the welded-on stiffeners would appear to be superior to copper-plating the cavities.

361-MeV (β = 0.710) Elliptical Cavities:
The conclusion from the two-dimensional analysis of the 361 MeV (β = 0.710) cavities and from review of the three-dimensional static and dynamic analyses of the β = 0.428 cavities is that the static and dynamic structural performance of the stiffened cavities will be no worse than, in fact better than, that of the β = 0.428 elliptical cavities.

VIII. RECOMMENDATIONS

It is recommended that the elliptical cavities for the superconducting concept of the APT linac be stiffened in the fashion described herein.

In the event that it is decided to proceed with the proposed APT SC RF Technology Demonstration, then resources should be provided to permit the determination of the static and dynamic structural characteristics of both single-cell and multi-cell cavities. This would involve further analysis of more complete models along with both static and dynamic testing.

In the event that there appears to be financial and/or technical benefit from extending the superconducting structure below 100 MeV, then more detailed analysis of lower energy ($\beta < 0.428$) cavities should be carried out. Following satisfactory predictions of the structural performance, resources should be provided to permit the experimental determination of the static and dynamic structural characteristics of both single-cell and multi-cell cavities at the lowest energy.

IX. ACKNOWLEDGMENTS

The authors hereby acknowledge support and advice from the following individuals:

Bob Gentzlinger for engineering design of the 4-cell cavities
Frank Krawczyk for MAFIA analysis of the cavities
Angela Naranjo for providing the 3-dimensional and cut-away views of the cavities
Brian Rusnak for review of the results relative to existing superconducting structures
Lloyd Young for SUPERFISH analysis of the half-cells

X. REFERENCES

I-1. T. Wangler, "Linear Accelerator for the Accelerator Production of Tritium, Design Challenges," Proc. of the 1990 Linear Accelerator Conference, Albuquerque, NM

I-2. D. Schrage et al, "Conceptual Design of a 7-MeV RFQ Linac for the Accelerator Production of Tritium," Los Alamos National Laboratory Report LA-UR-93-1790

I-3. J. Billen, "A New Accelerator Structure for Intermediate-Velocity Particles, "Proc. Of the 1994 Linear Accelerator Conference, Tsukuba, Japan

I-4. E. Knapp et al, "Accelerating Structure Research at Los Alamos," Proc. Of the 1966 Linear Accelerator Conference, Santa Fe, NM

I-5. B. Rusnak & A. Shapiro, "Test Results of a Heat-Treated 4-Cell 805 MHz Superconducting Cavity," 1995 Particle Accelerator Conference, May 1995, Dallas

II-1. M. G. Rao & P. Kneissel, "Mechanical and Thermal Properties of High RRR Niobium at Cryogenic Temperatures," CEBAF Technical Note #0097 (1988)

IV-1. A. Matziali & H. Schwettman, "Vibrational Analysis of the TESLA Structure," Proc. of the 6th Workshop on RF Superconductivity," 1993, CEBAF

IV-2. S. Simrock, "Experience with Control of Frequency, Amplitude, and Phase," Proceedings of the 6th Workshop on RF Superconductivity, CEBAF (1993)

IV-3. D. Schrage, "Fabrication Technology Development for Low β Elliptical Cavities," memo, AT-1:93-102, April 1993

IV-4. C. Arnaud et al, "Status Report on Superconducting Niobium Cavities for LEP," Proceedings of the 4th Workshop on RF Superconductivity, KEK (1989)

Figure I-1

LOS ALAMOS NATIONAL LABORATORY

100 MeV (β=0.43) 4-CELL 700 MHz
SUPERCONDUCTING CAVITY
for the
ACCELERATOR PRODUCTION OF TRITIUM

PRELIMINARY CONCEPT JULY 1995

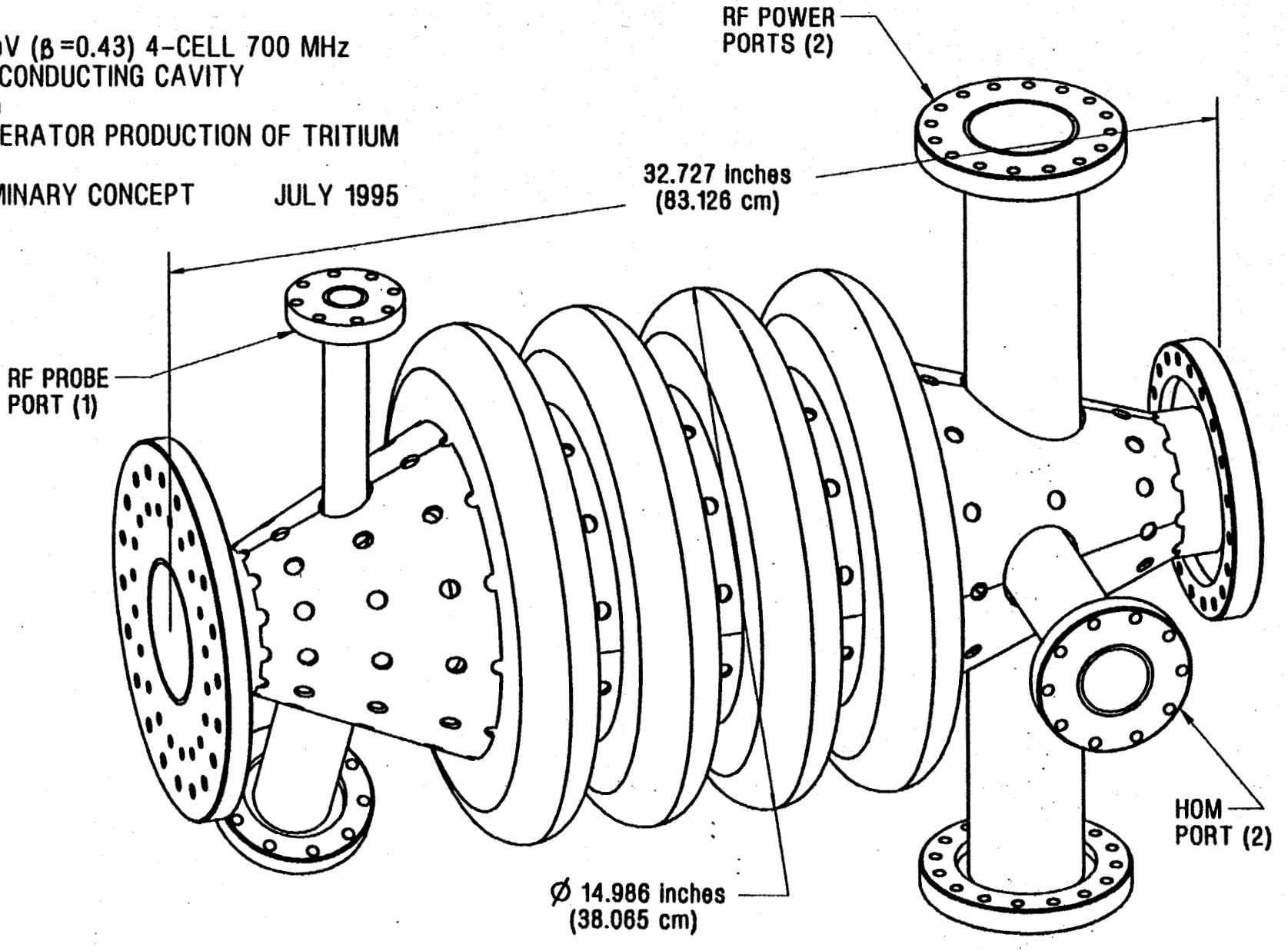

APT SUPERCONDUCTING LINAC CAVITY CROSS-SECTIONS

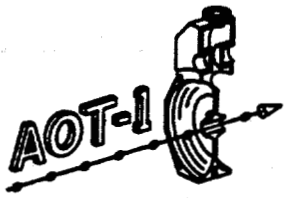

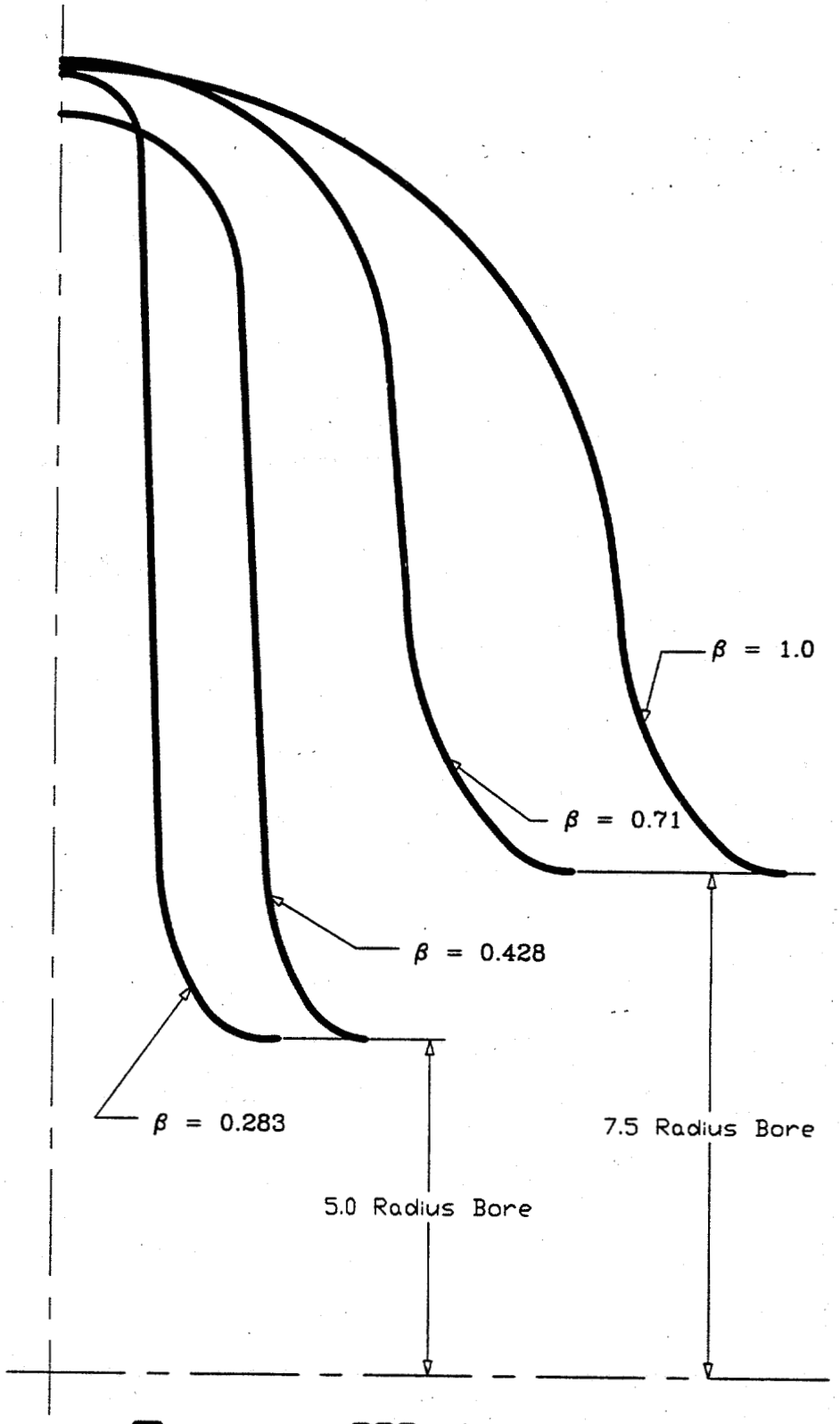

Figure III-1 FULL SCALE

APT SUPERCONDUCTING LINAC
100 MeV HALF-CELL

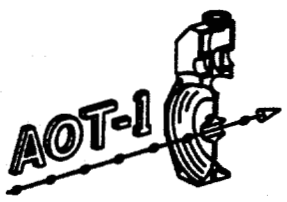

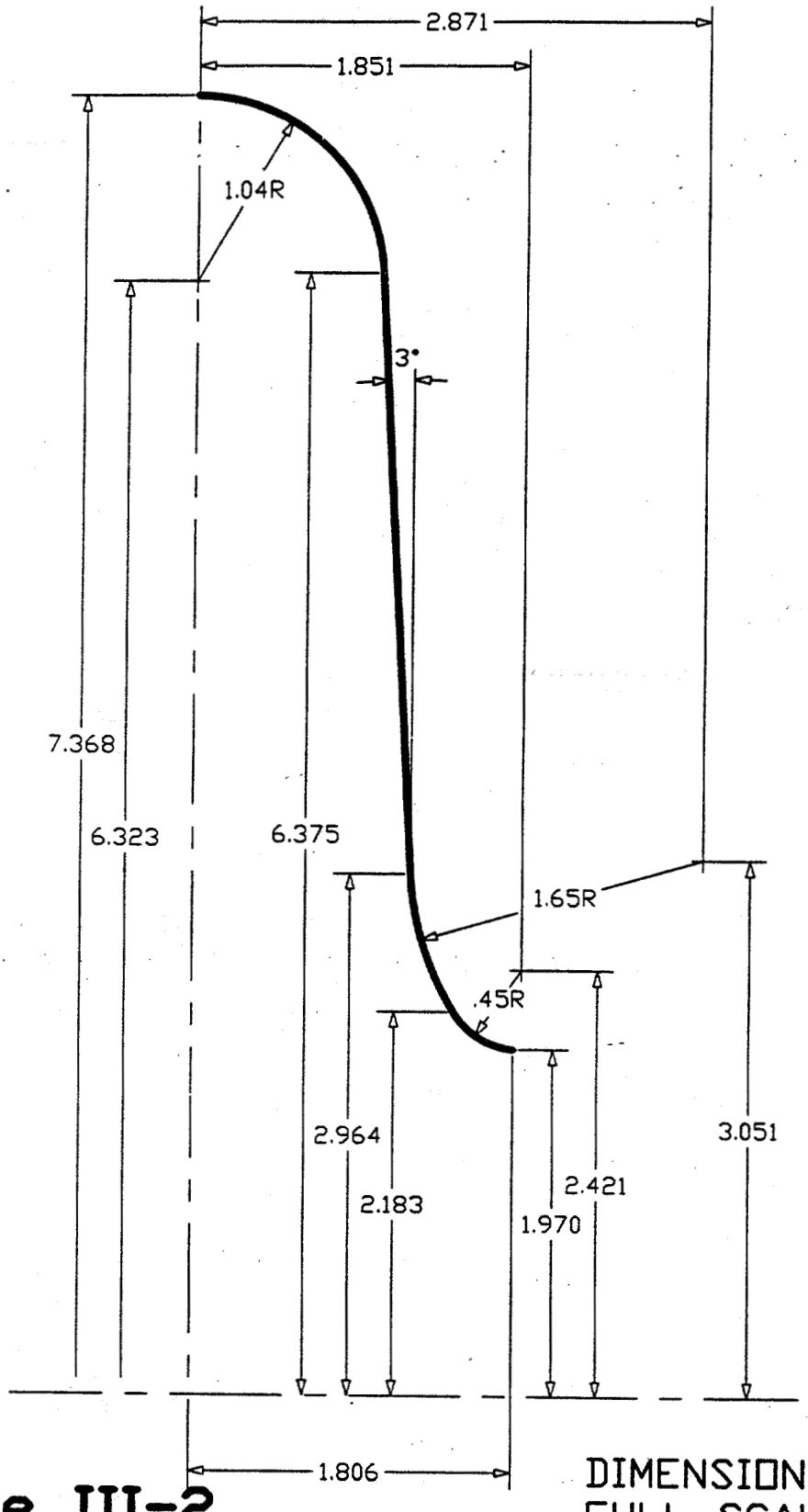

Figure III-2

DIMENSIONS IN INCHES
FULL SCALE

APT SUPERCONDUCTING LINAC
361 MeV HALF-CELL

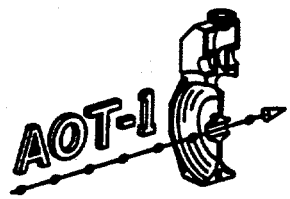

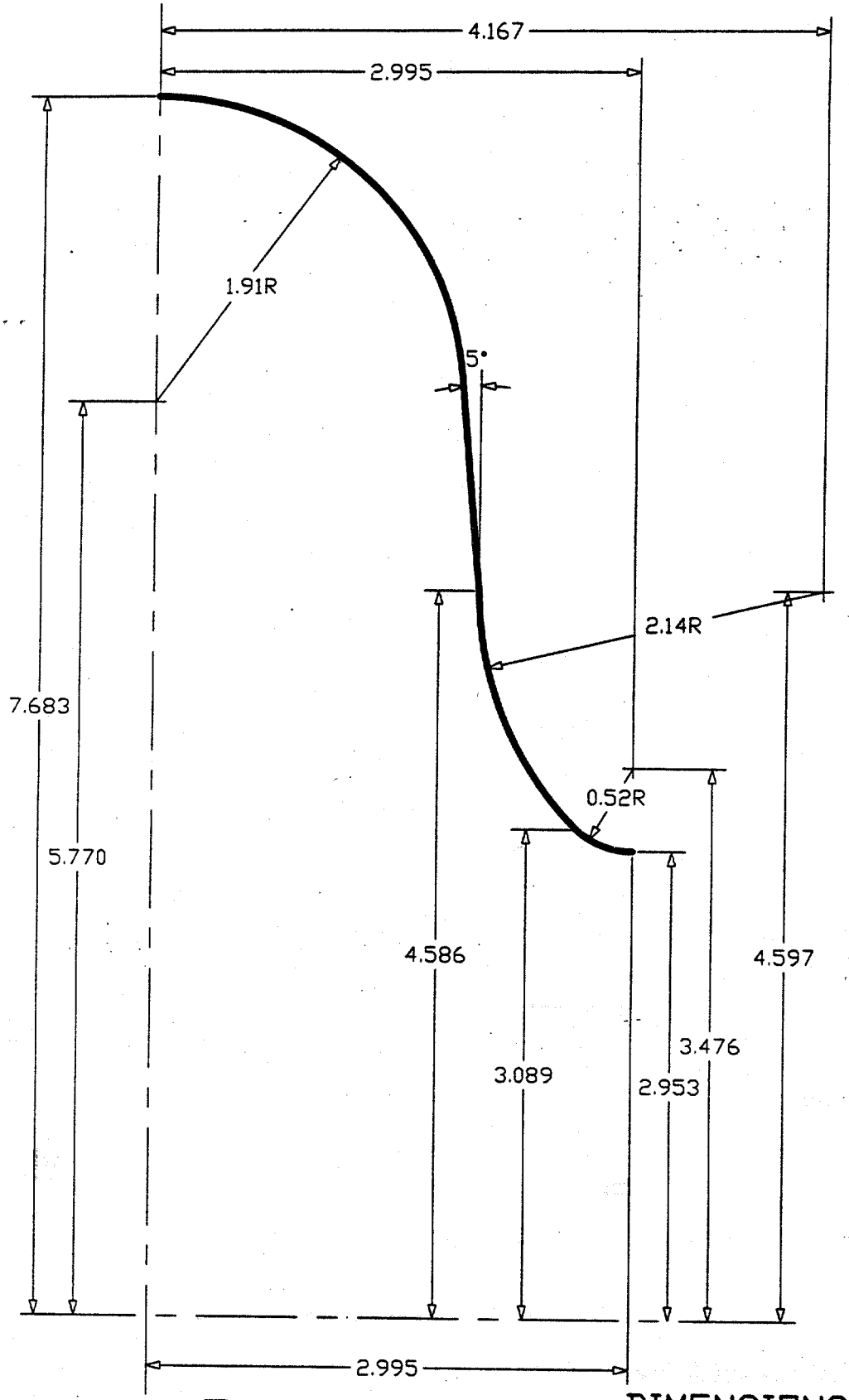

Figure III-3

DIMENSIONS IN INCHES
FULL SCALE

APT SUPERCONDUCTING LINAC
40 MeV HALF-CELL

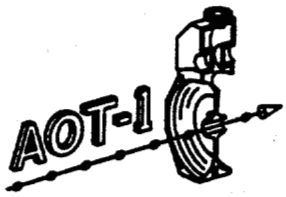

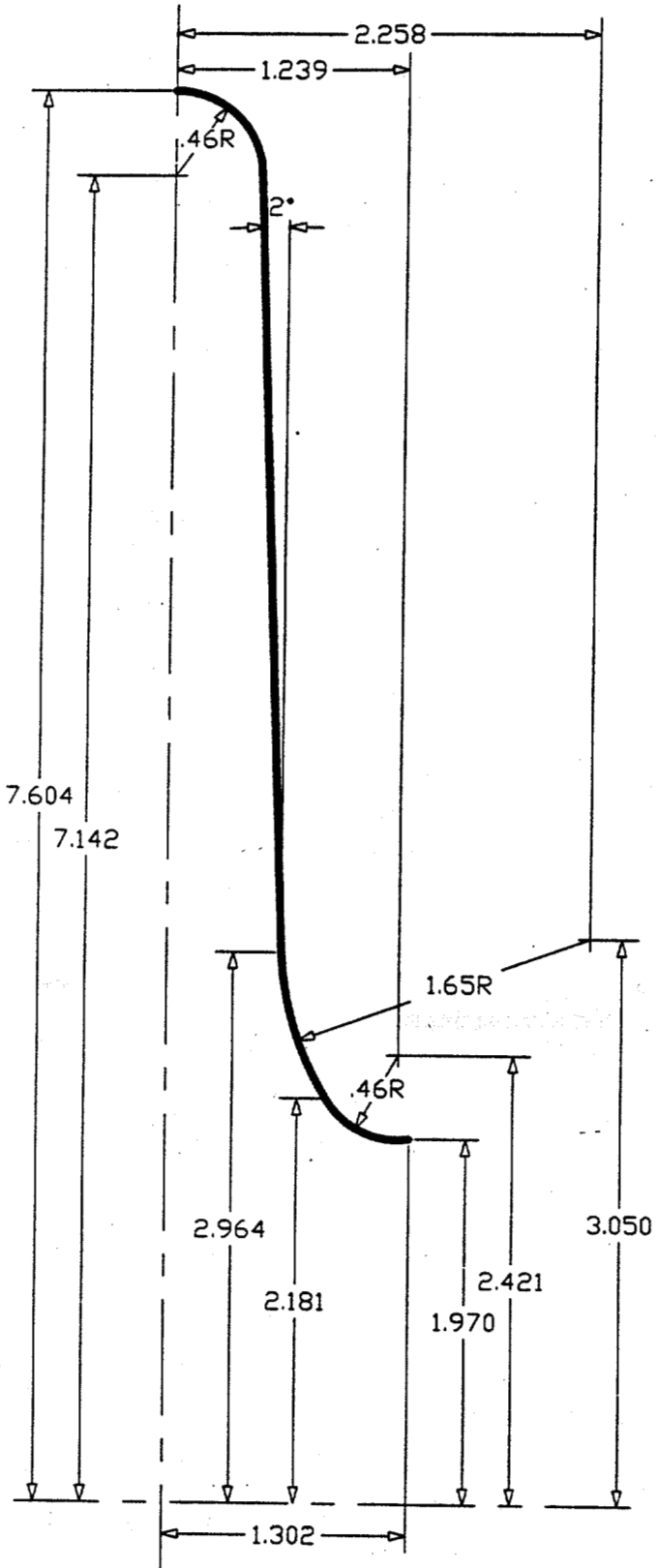

Figure III-4

DIMENSIONS IN INCHES
FULL SCALE

APT SUPERCONDUCTING LINAC

$\beta = 1$ HALF-CELL

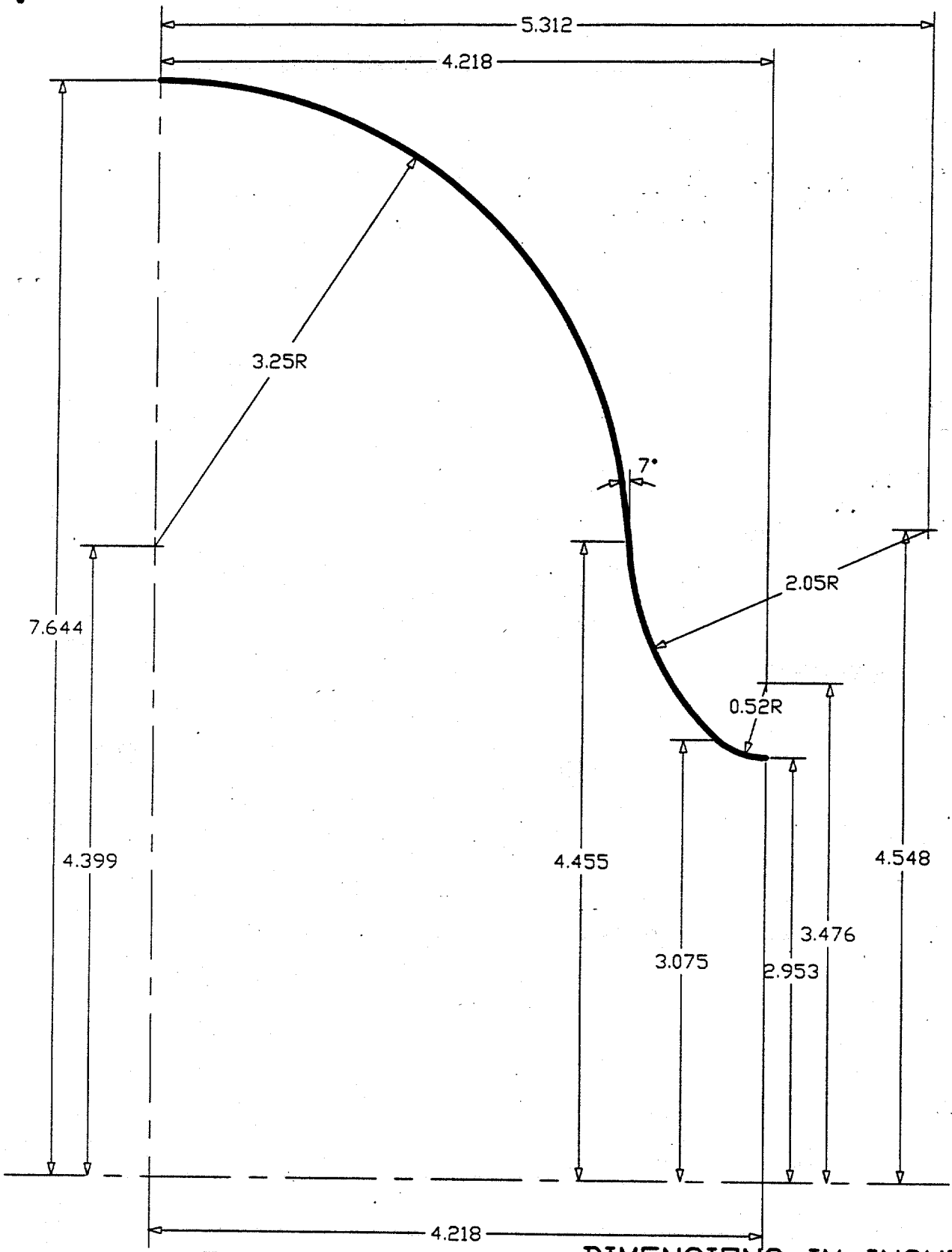

Figure III-5

DIMENSIONS IN INCHES
FULL SCALE

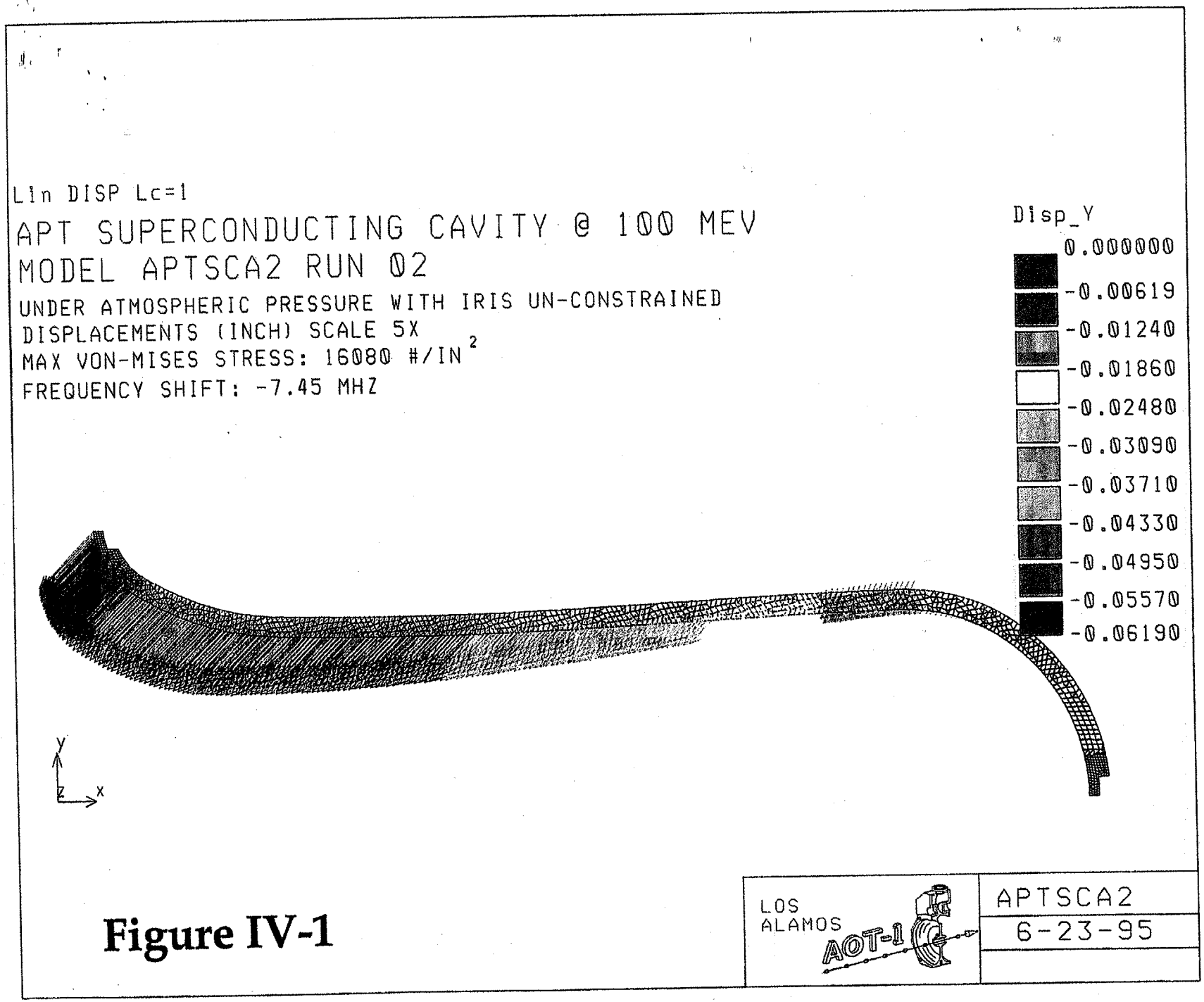
Lin DISP Lc=1
APT SUPERCONDUCTING CAVITY @ 100 MEV
MODEL APTSCA2 RUN 02
UNDER ATMOSPHERIC PRESSURE WITH IRIS UN-CONSTRAINED
DISPLACEMENTS (INCH) SCALE 5X
MAX VON-MISES STRESS: 16080 #/IN 2
FREQUENCY SHIFT: -7.45 MHZ
Disp_Y
0.000000
-0.00619
-0.01240
-0.01860
-0.02480
-0.03090
-0.03710
-0.04330
-0.04950
-0.05570
-0.06190
Y
Z
X
LOS ALAMOS
AOT-1
APTSCA2
6-23-95

Figure IV-1

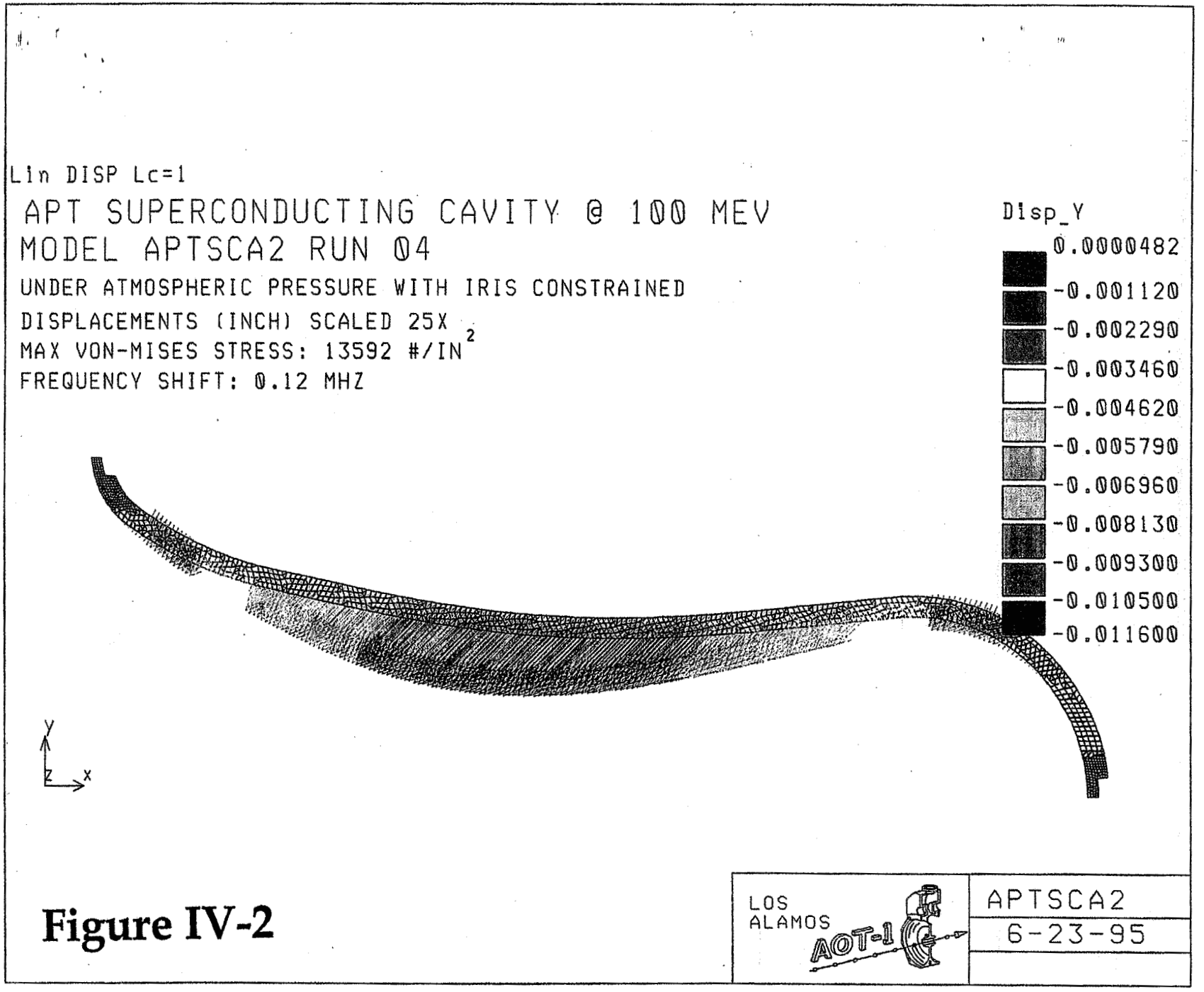
Lin DISP Lc=1
APT SUPERCONDUCTING CAVITY @ 100 MEV
MODEL APTSCA2 RUN 04
UNDER ATMOSPHERIC PRESSURE WITH IRIS CONSTRAINED
DISPLACEMENTS (INCH) SCALED 25X
MAX VON-MISES STRESS: 13592 #/IN2
FREQUENCY SHIFT: 0.12 MHZ
Disp_Y
0.0000482
-0.001120
-0.002290
-0.003460
-0.004620
-0.005790
-0.006960
-0.008130
-0.009300
-0.010500
-0.011600
Y
Z
X
LOS ALAMOS
AOT-1
APTSCA2
6-23-95

Figure IV-2

Figure IV-3

LOS ALAMOS NATIONAL LABORATORY

100 MeV (β=0.43) 4-CELL 700 MHz
SUPERCONDUCTING CAVITY
for the
ACCELERATOR PRODUCTION OF TRITIUM

EXPLODED VIEW OF
PRELIMINARY CONCEPT JULY 1995

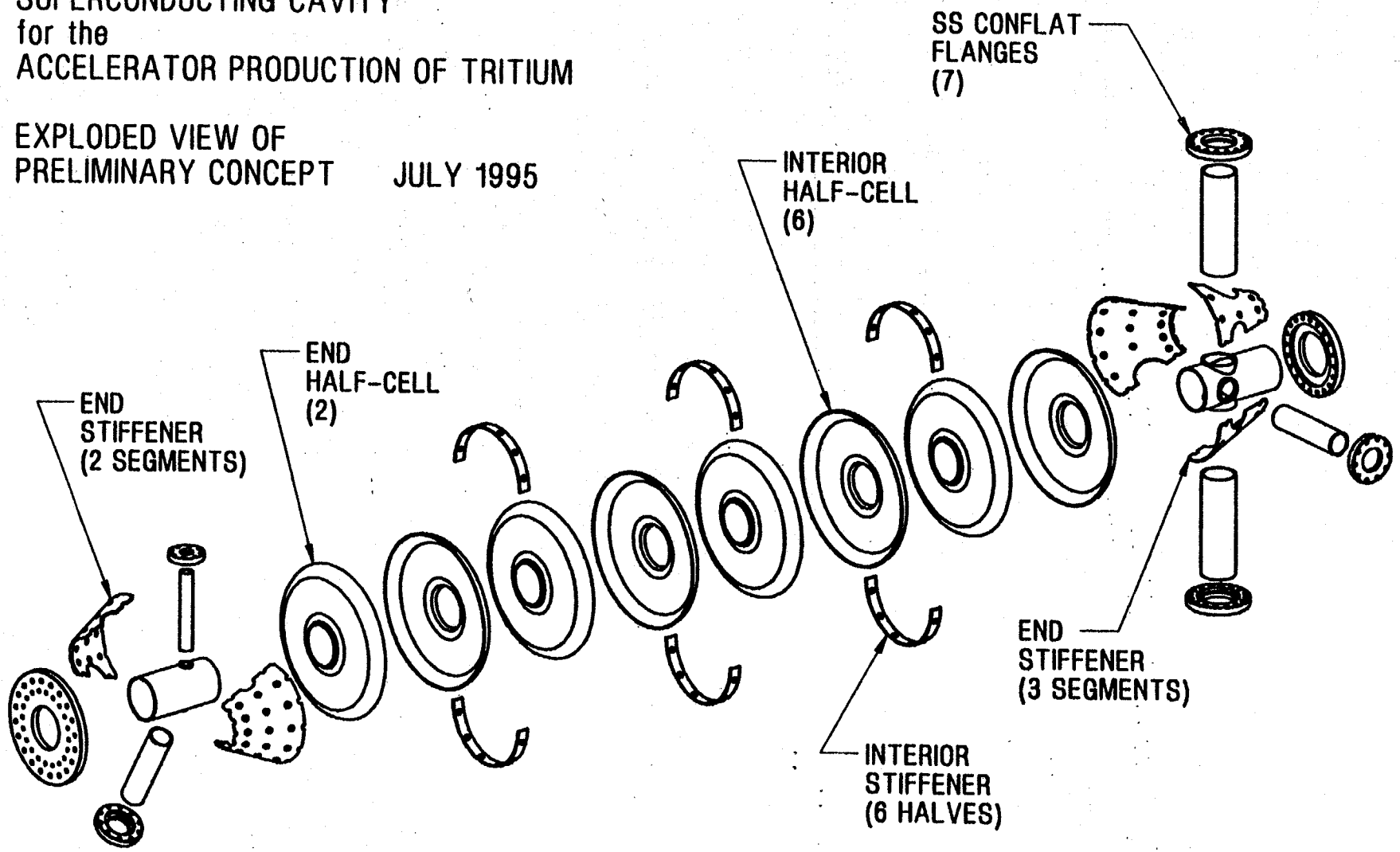

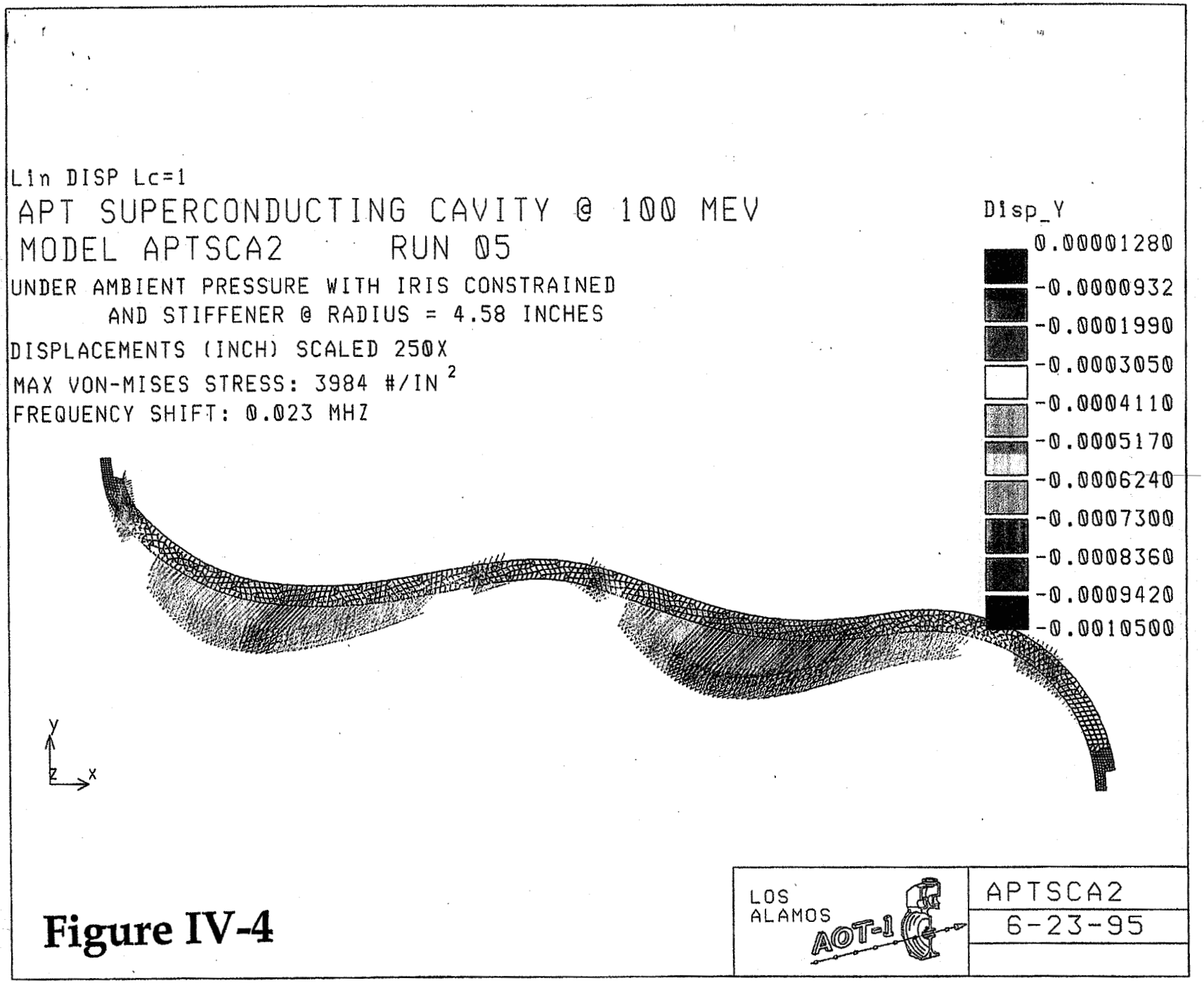
Lin DISP Lc=1
APT SUPERCONDUCTING CAVITY @ 100 MEV
MODEL APTSCA2 RUN 05
UNDER AMBIENT PRESSURE WITH IRIS CONSTRAINED
AND STIFFENER @ RADIUS = 4.58 INCHES
DISPLACEMENTS (INCH) SCALED 250X
MAX VON-MISES STRESS: 3984 #/IN 2
FREQUENCY SHIFT: 0.023 MHZ
Disp_Y
0.00001280
-0.0000932
-0.0001990
-0.0003050
-0.0004110
-0.0005170
-0.0006240
-0.0007300
-0.0008360
-0.0009420
-0.0010500
y
z
x
LOS ALAMOS
AOT-1
APTSCA2
6-23-95

Figure IV-4

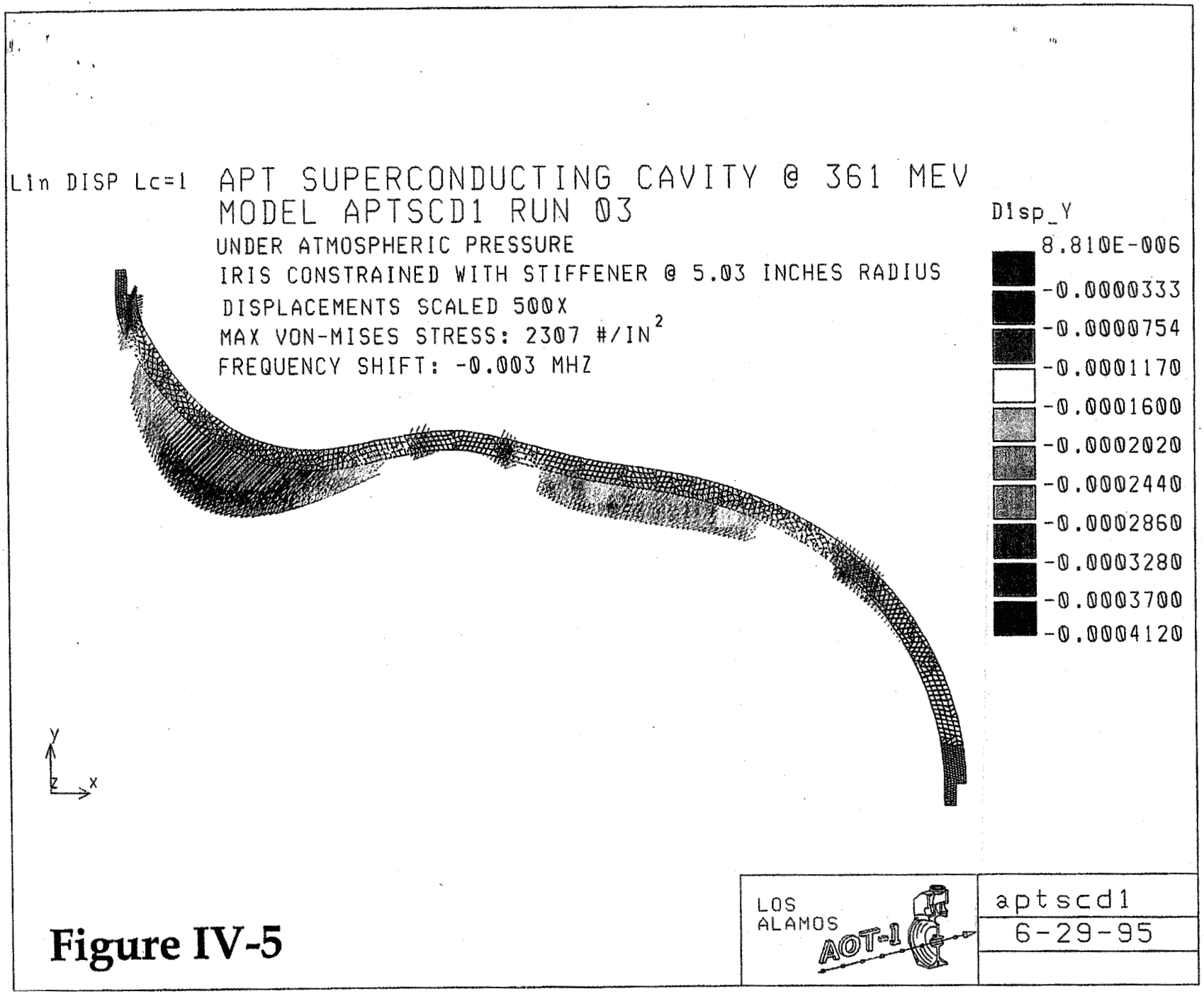
Lin DISP Lc=1
APT SUPERCONDUCTING CAVITY @ 361 MEV
MODEL APTSCD1 RUN 03
UNDER ATMOSPHERIC PRESSURE
IRIS CONSTRAINED WITH STIFFENER @ 5.03 INCHES RADIUS
DISPLACEMENTS SCALED 500X
MAX VON-MISES STRESS: 2307 #/IN2
FREQUENCY SHIFT: -0.003 MHZ
Disp_Y
8.810E-006
-0.0000333
-0.0000754
-0.0001170
-0.0001600
-0.0002020
-0.0002440
-0.0002860
-0.0003280
-0.0003700
-0.0004120
Y
Z
X
LOS ALAMOS
AOT-1
aptscd1
6-29-95

Figure IV-5

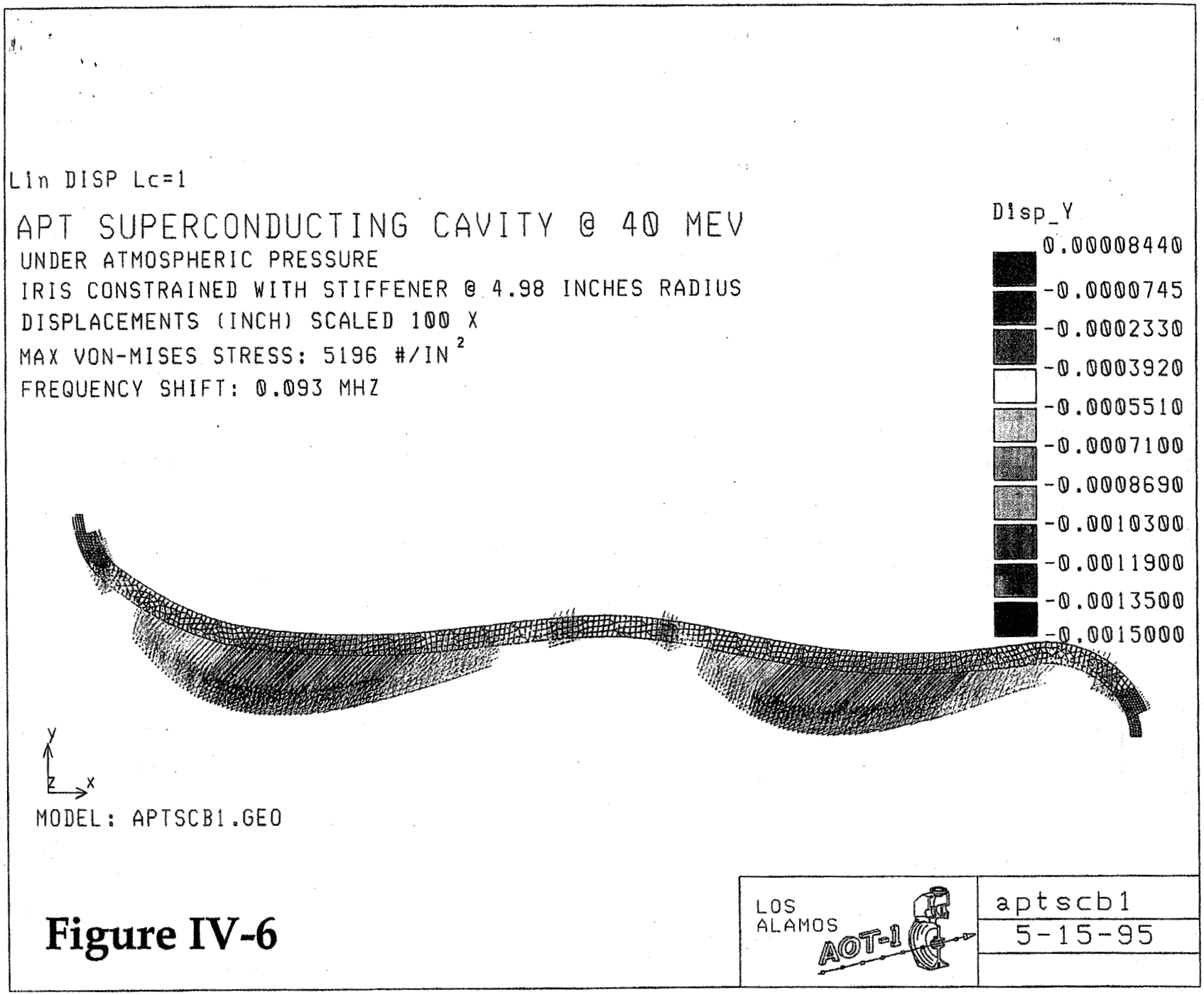
Lin DISP Lc=1
APT SUPERCONDUCTING CAVITY @ 40 MEV
UNDER ATMOSPHERIC PRESSURE
IRIS CONSTRAINED WITH STIFFENER @ 4.98 INCHES RADIUS
DISPLACEMENTS (INCH) SCALED 100 X
MAX VON-MISES STRESS: 5196 #/IN 2
FREQUENCY SHIFT: 0.093 MHZ
Disp_Y
0.00008440
-0.0000745
-0.0002330
-0.0003920
-0.0005510
-0.0007100
-0.0008690
-0.0010300
-0.0011900
-0.0013500
-0.0015000
Y
Z
X
MODEL: APTSCB1.GEO
LOS ALAMOS
AOT-1
aptscb1
5-15-95

Figure IV-6

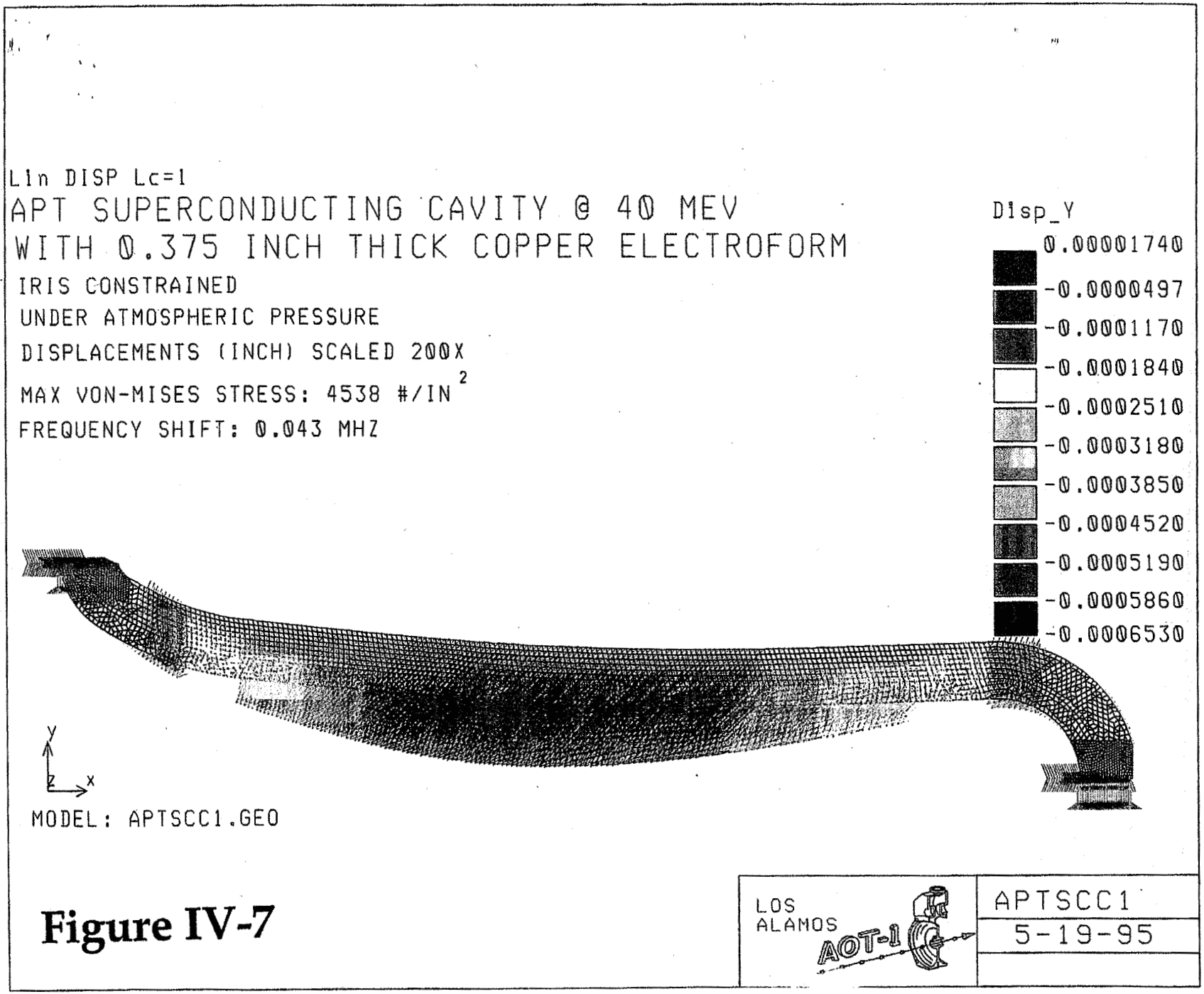
Lin DISP Lc=1
APT SUPERCONDUCTING CAVITY @ 40 MEV
WITH 0.375 INCH THICK COPPER ELECTROFORM
IRIS CONSTRAINED
UNDER ATMOSPHERIC PRESSURE
DISPLACEMENTS (INCH) SCALED 200X
MAX VON-MISES STRESS: 4538 #/IN 2
FREQUENCY SHIFT: 0.043 MHZ
Disp_Y
0.00001740
-0.0000497
-0.0001170
-0.0001840
-0.0002510
-0.0003180
-0.0003850
-0.0004520
-0.0005190
-0.0005860
-0.0006530
y
z
x
MODEL: APTSCC1.GEO
LOS ALAMOS
AOT-1
APTSCC1
5-19-95

Figure IV-7

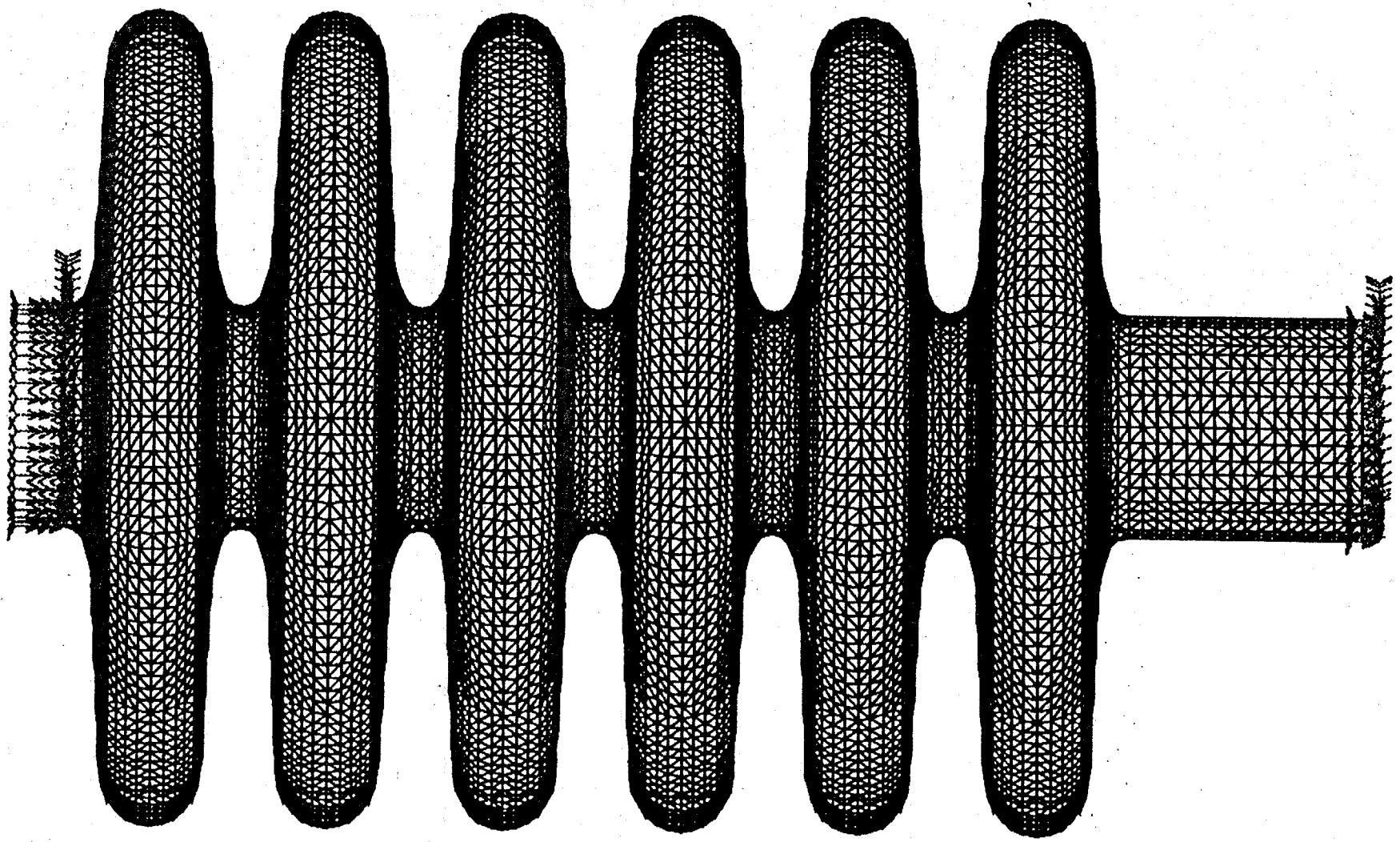

Figure V-1: Finite Element Model of the 6-Cell Cavity.

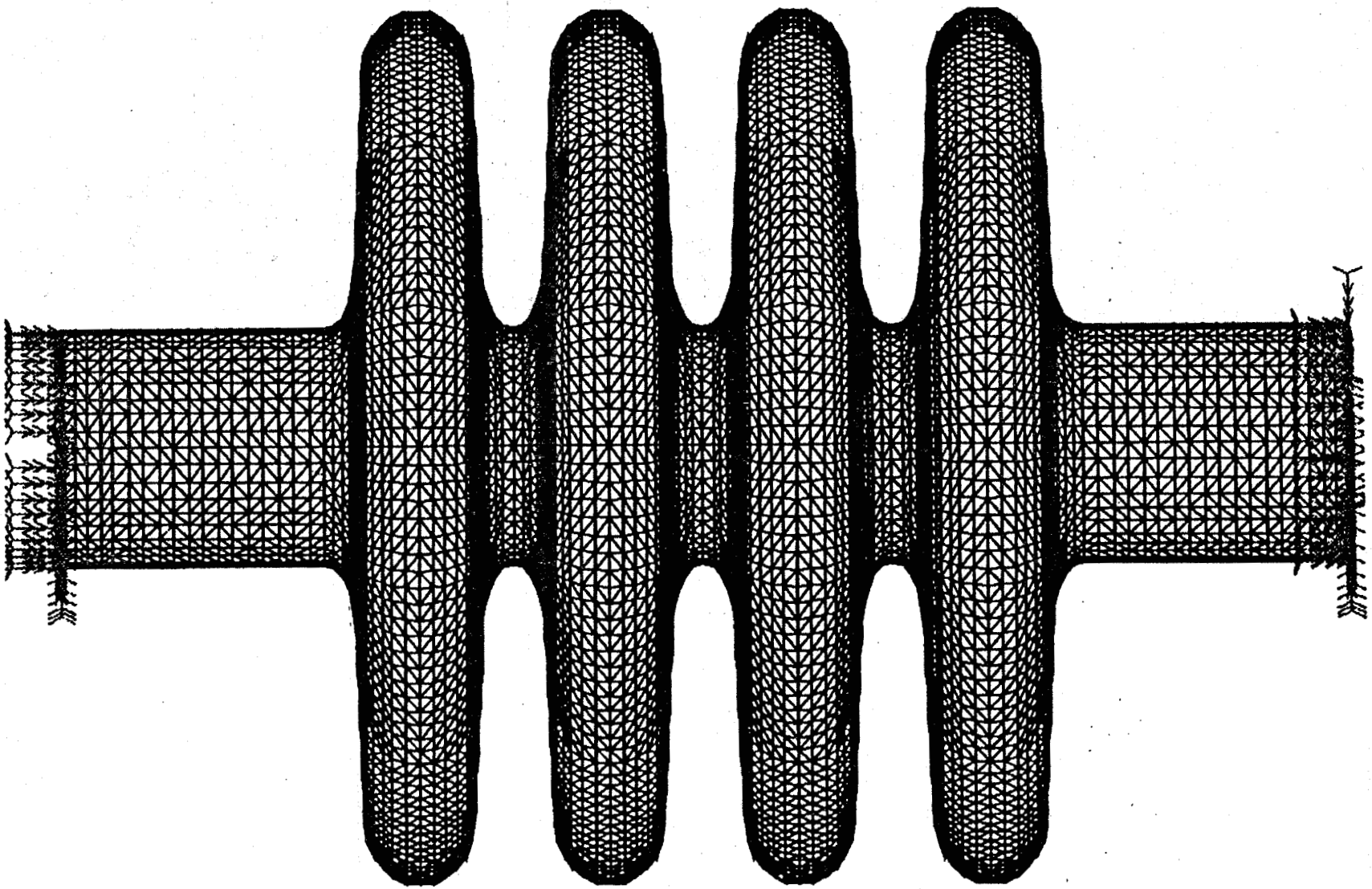

Figure V-2: Finite Element Model of the 4-Cell Cavity.

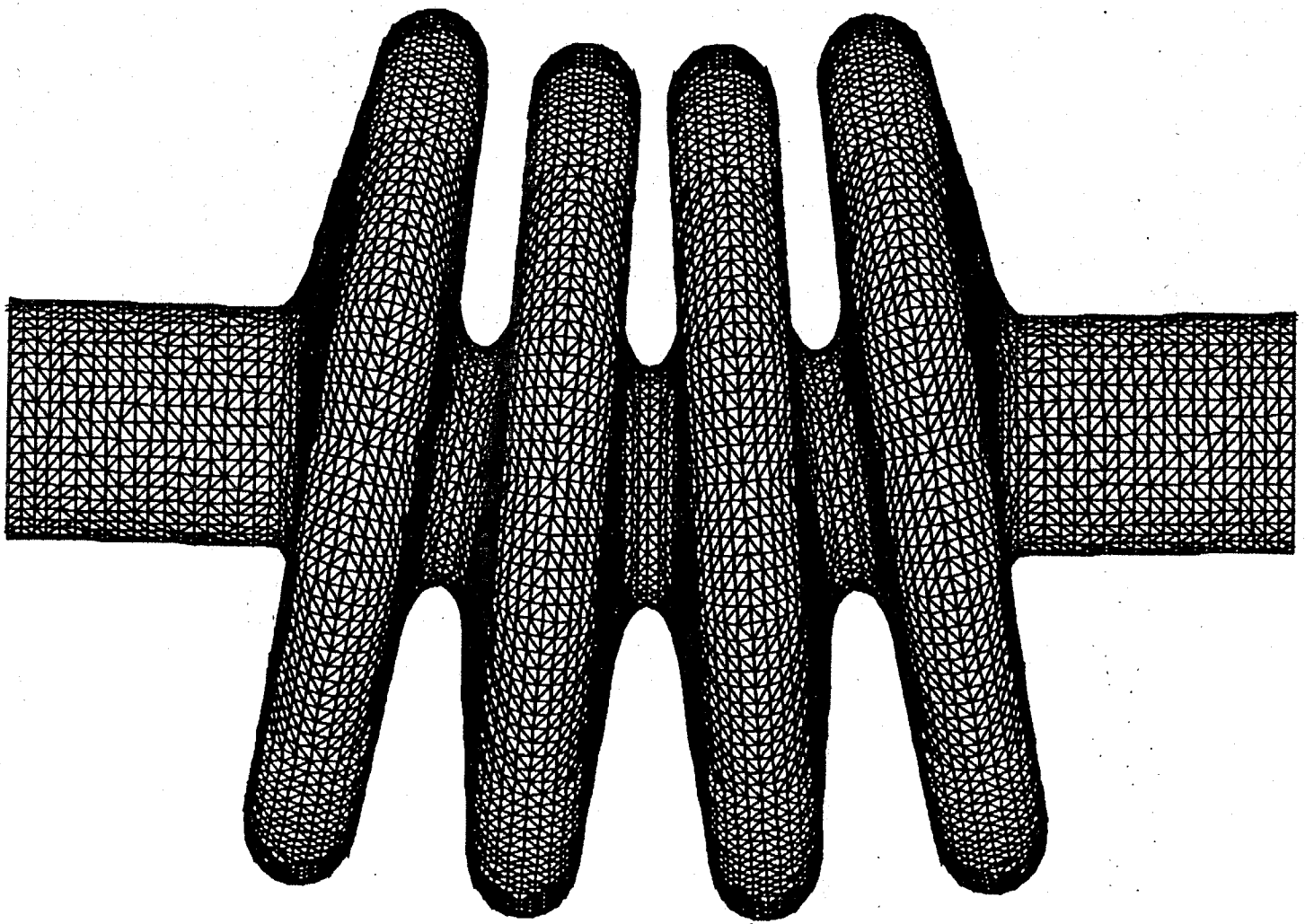

Figure V-3: Transverse Deformations that Result from the Transverse Gravitational Load

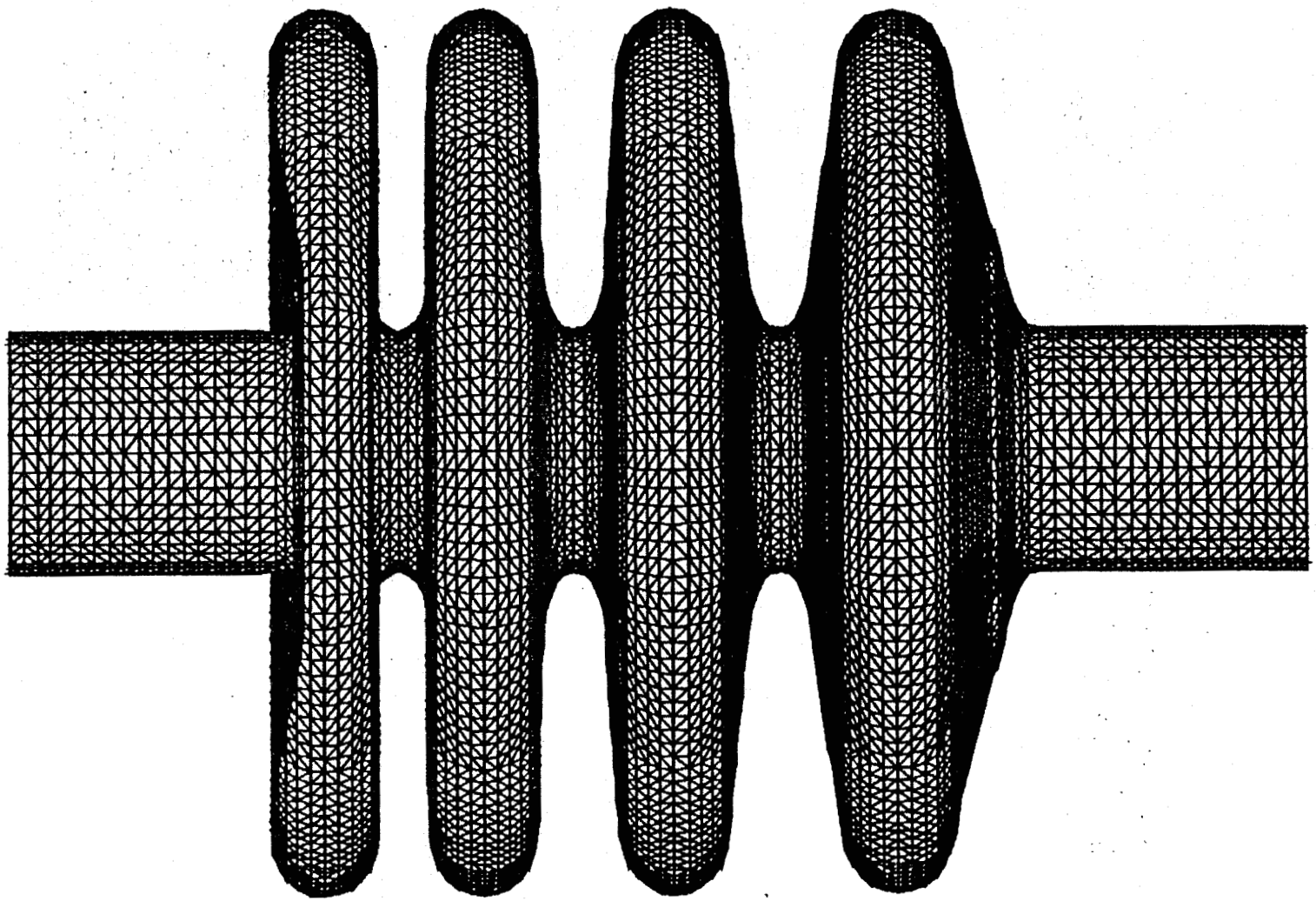

Figure V-4: Axial Deformations that Result from the Axial Gravitational Load

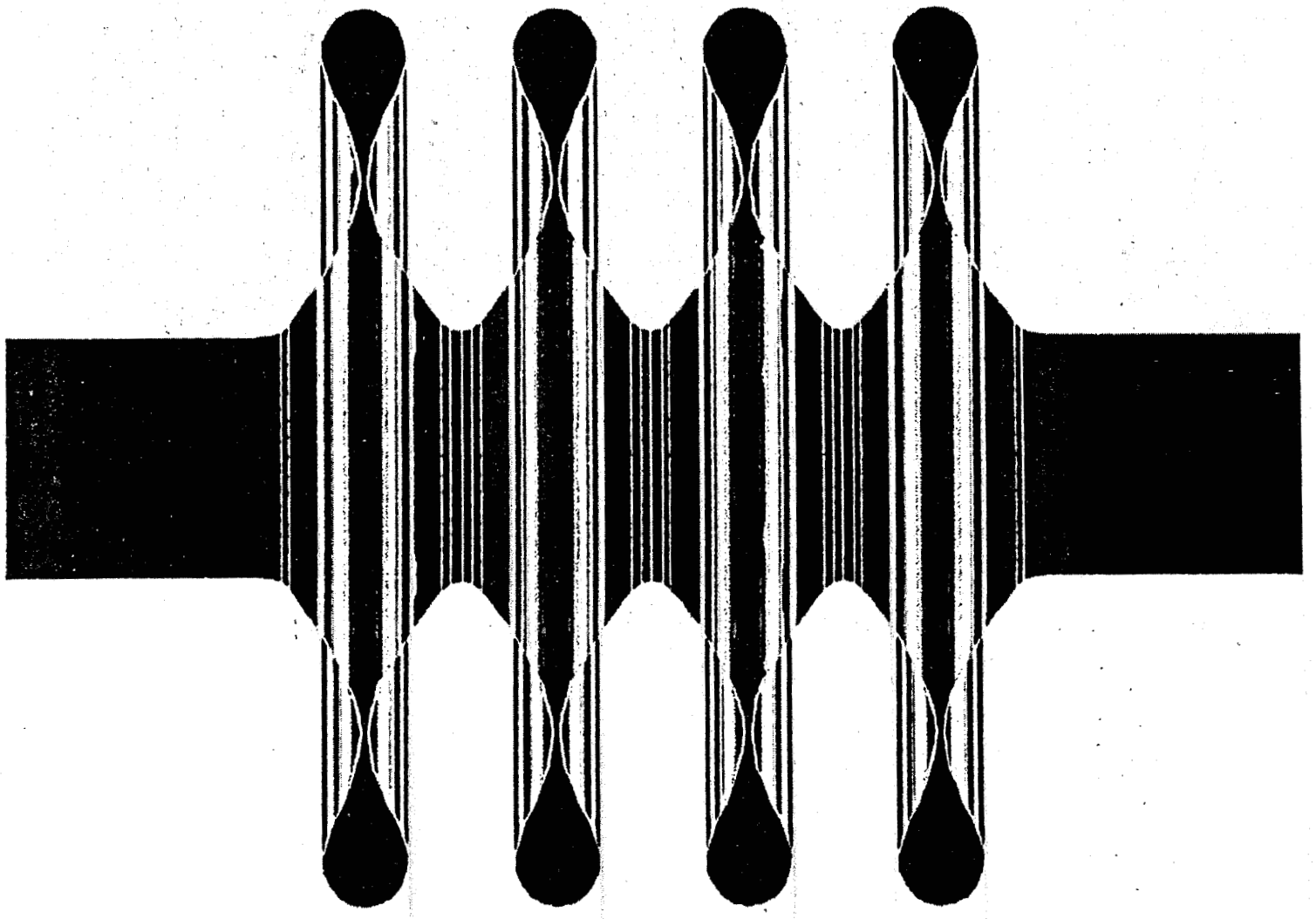

Figure V-5: Axial Deformations that Result from the Ambient Pressure Load

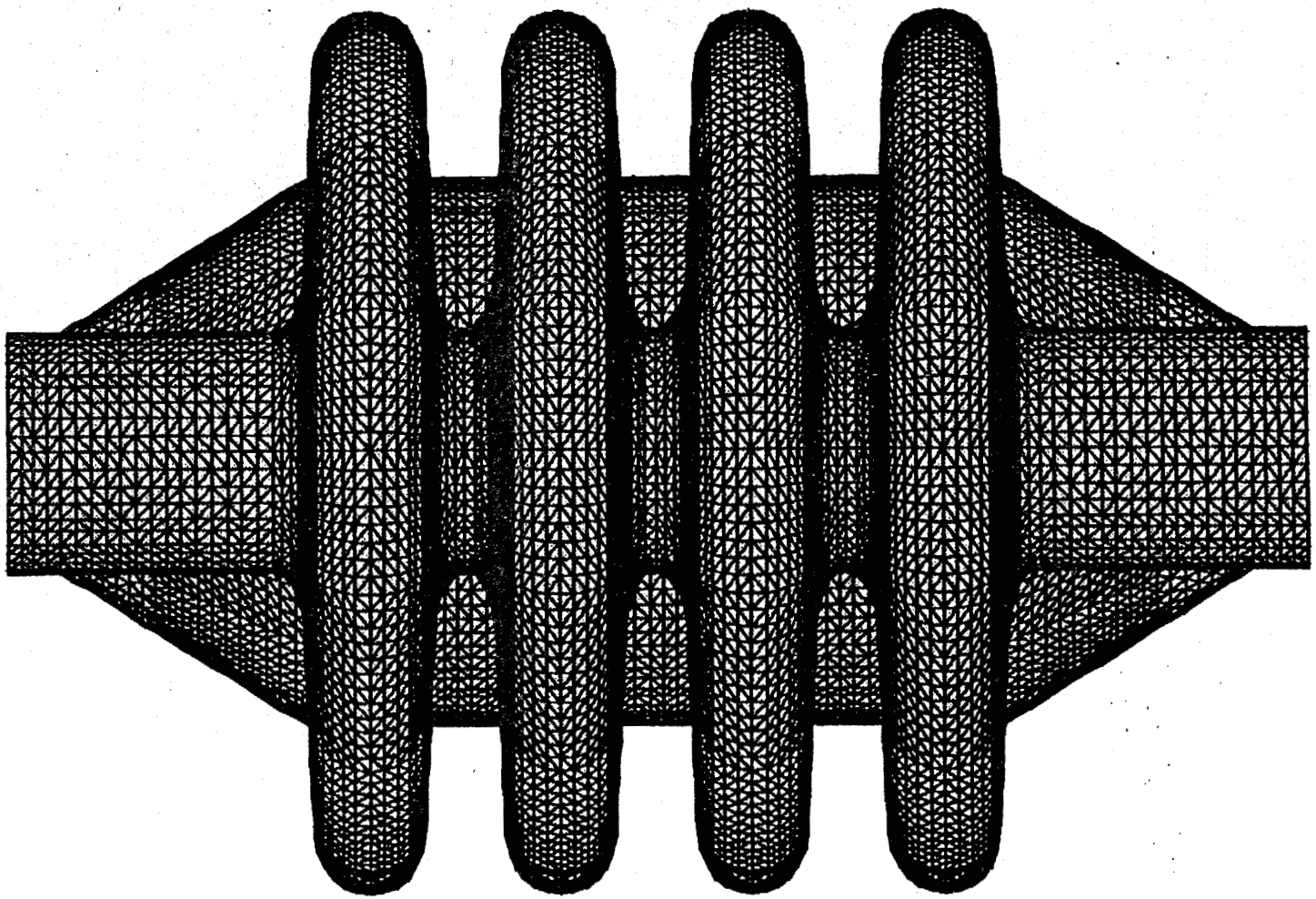

Figure V-6: Cross-Section of the Radial and Cylindrical Stiffeners Used on the 4-Cell Cavity

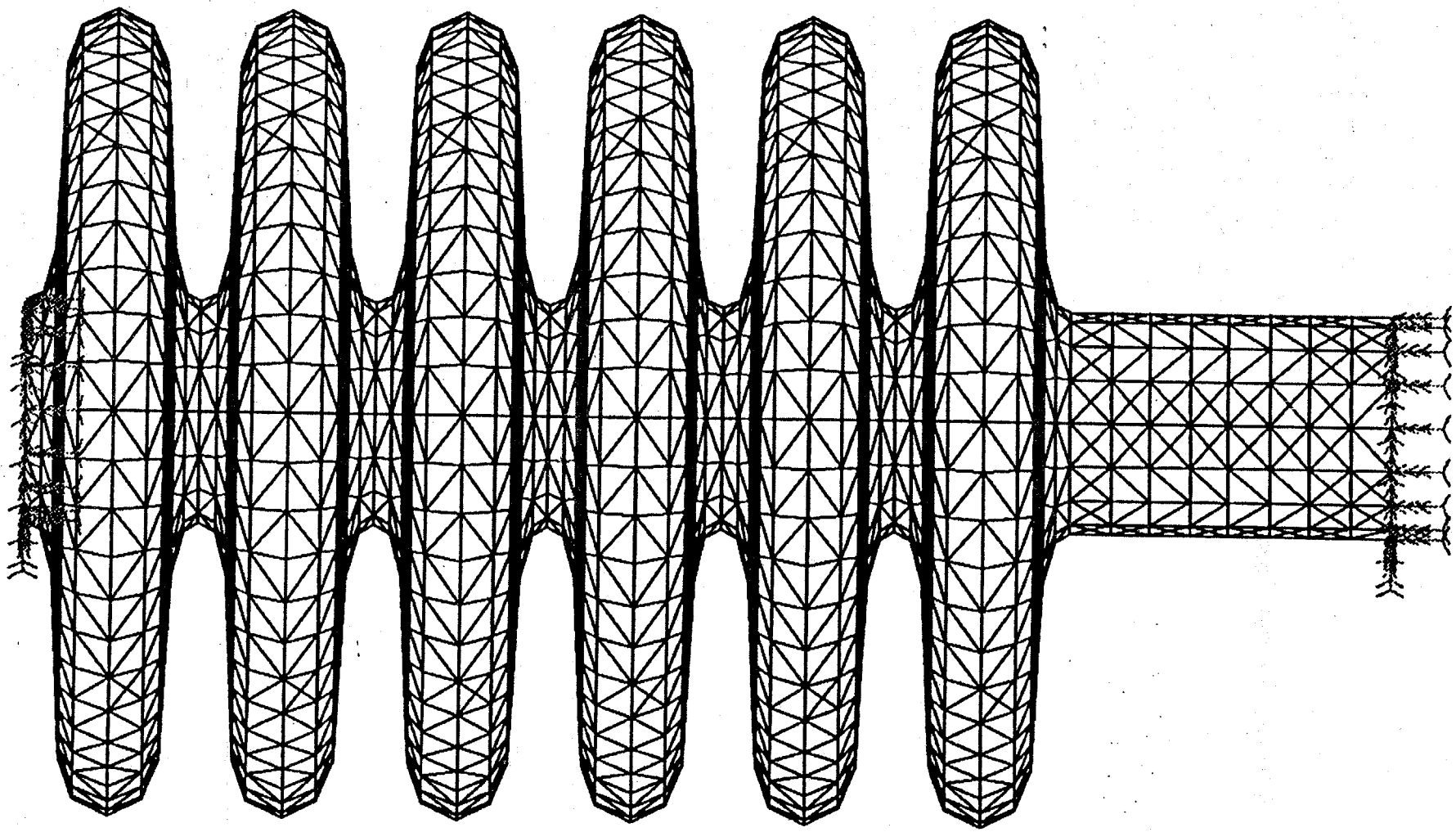

Figure VI-1: Finite Element Model of the 6-Cell Cavity for Dynamic Analysis

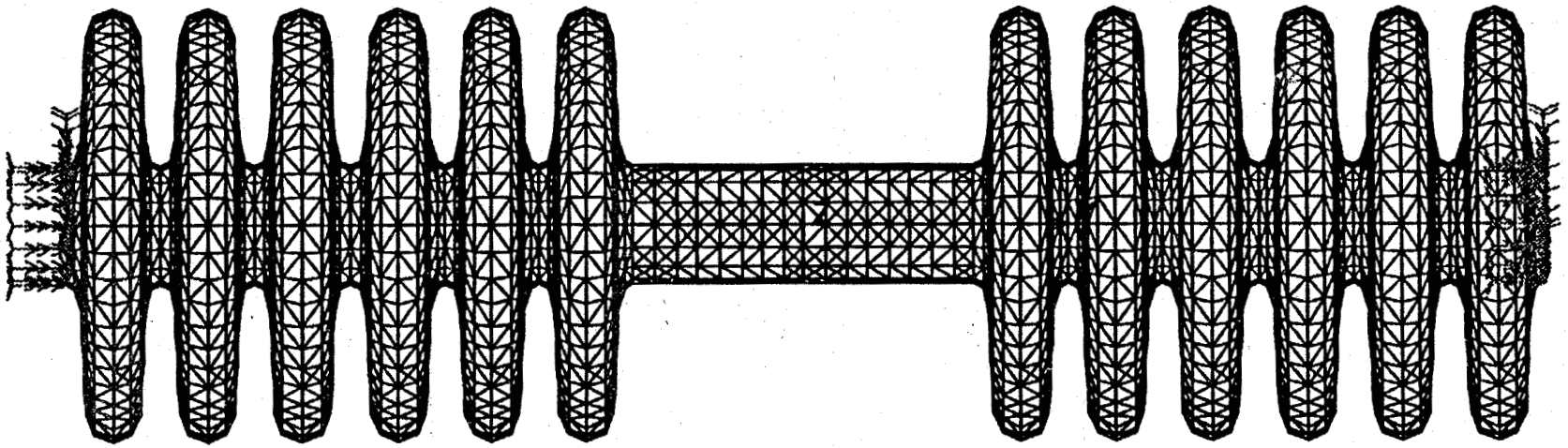

Figure VI-2: Finite Element Model of the 12-Cell Cavity for Dynamic Analysis

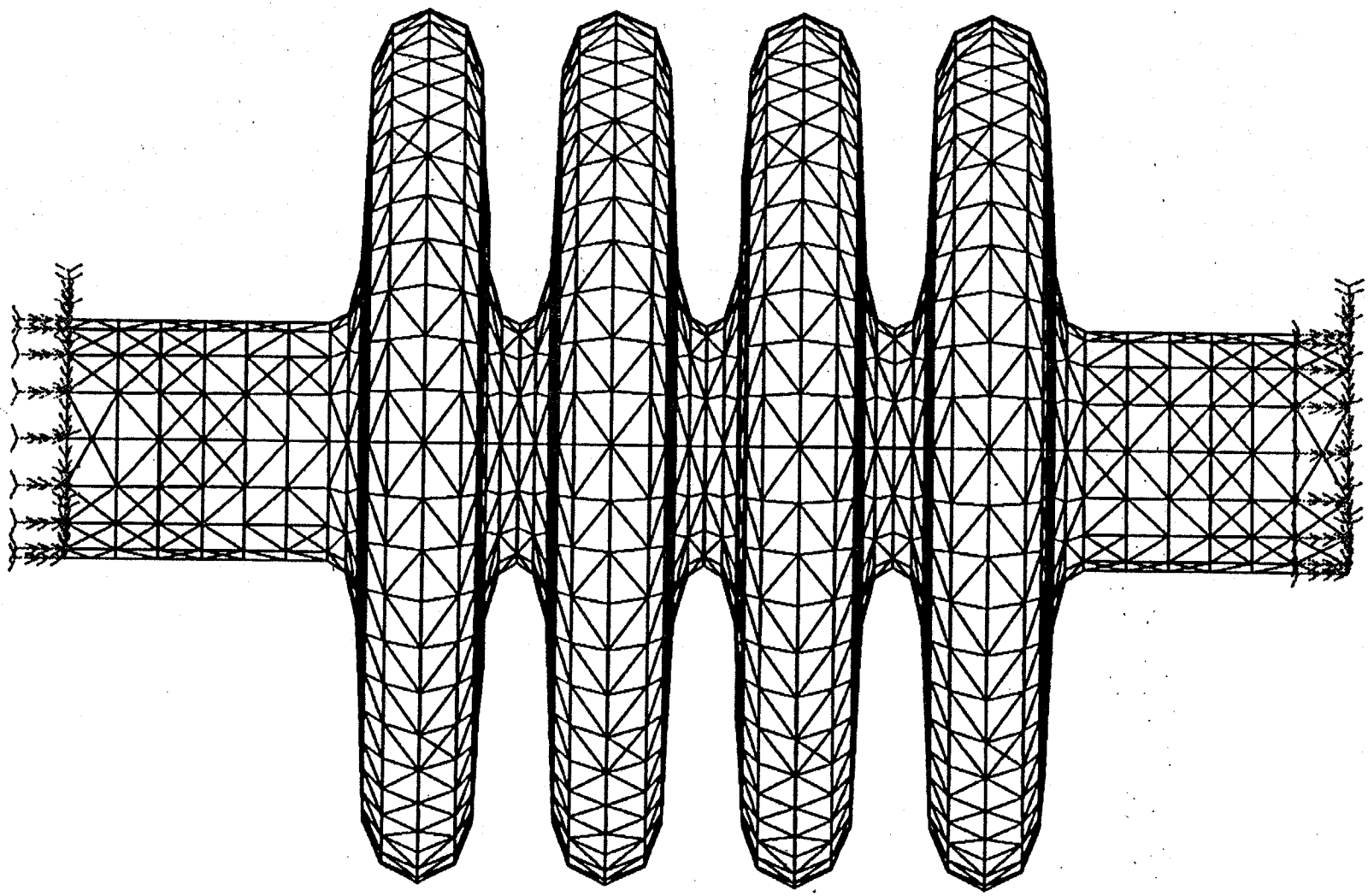

Figure VI-3: Finite Element Model of the 4-Cell Cavity for Dynamic Analysis

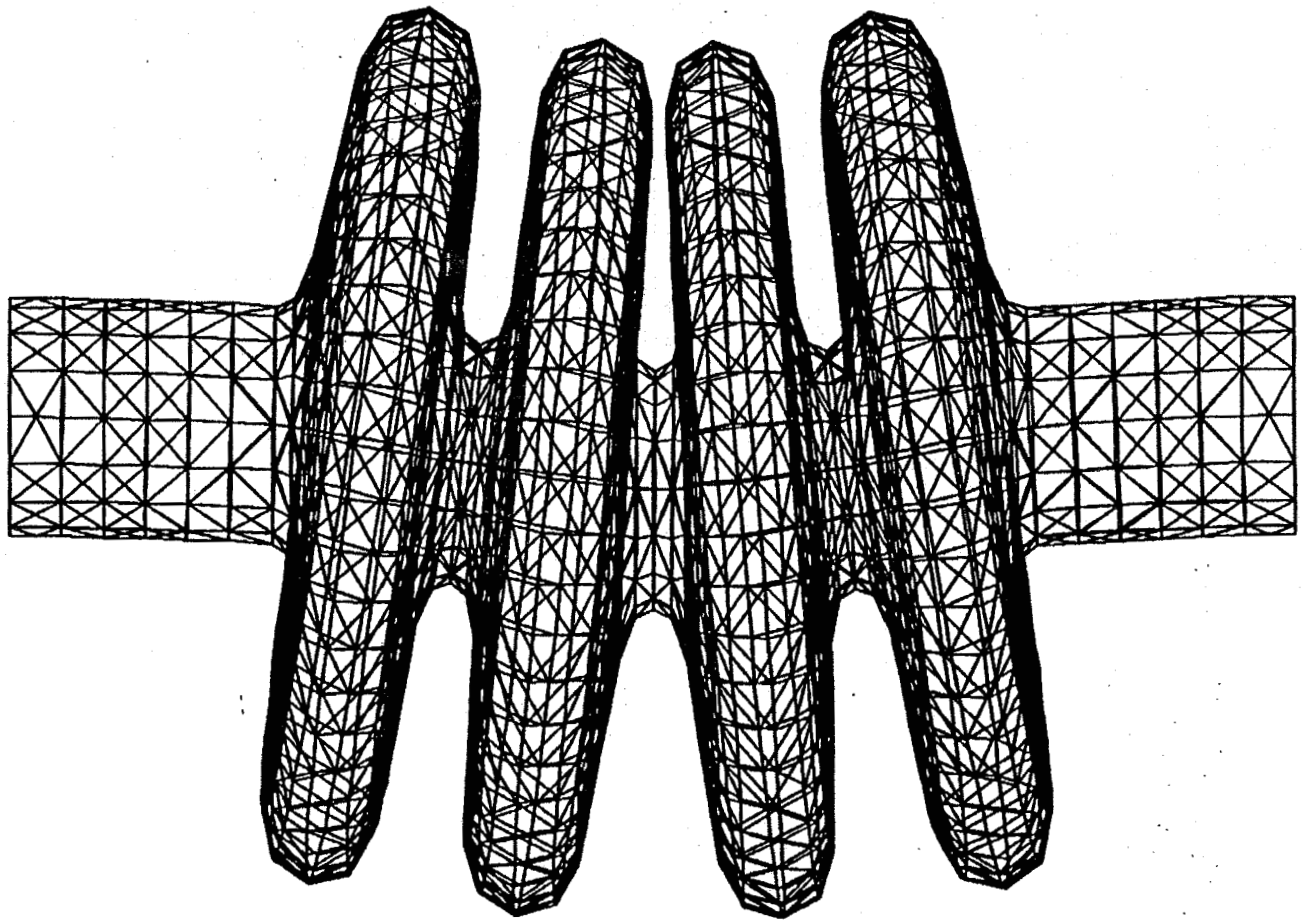

Figure VI-4: Finite Element Model of the First Transverse Mode

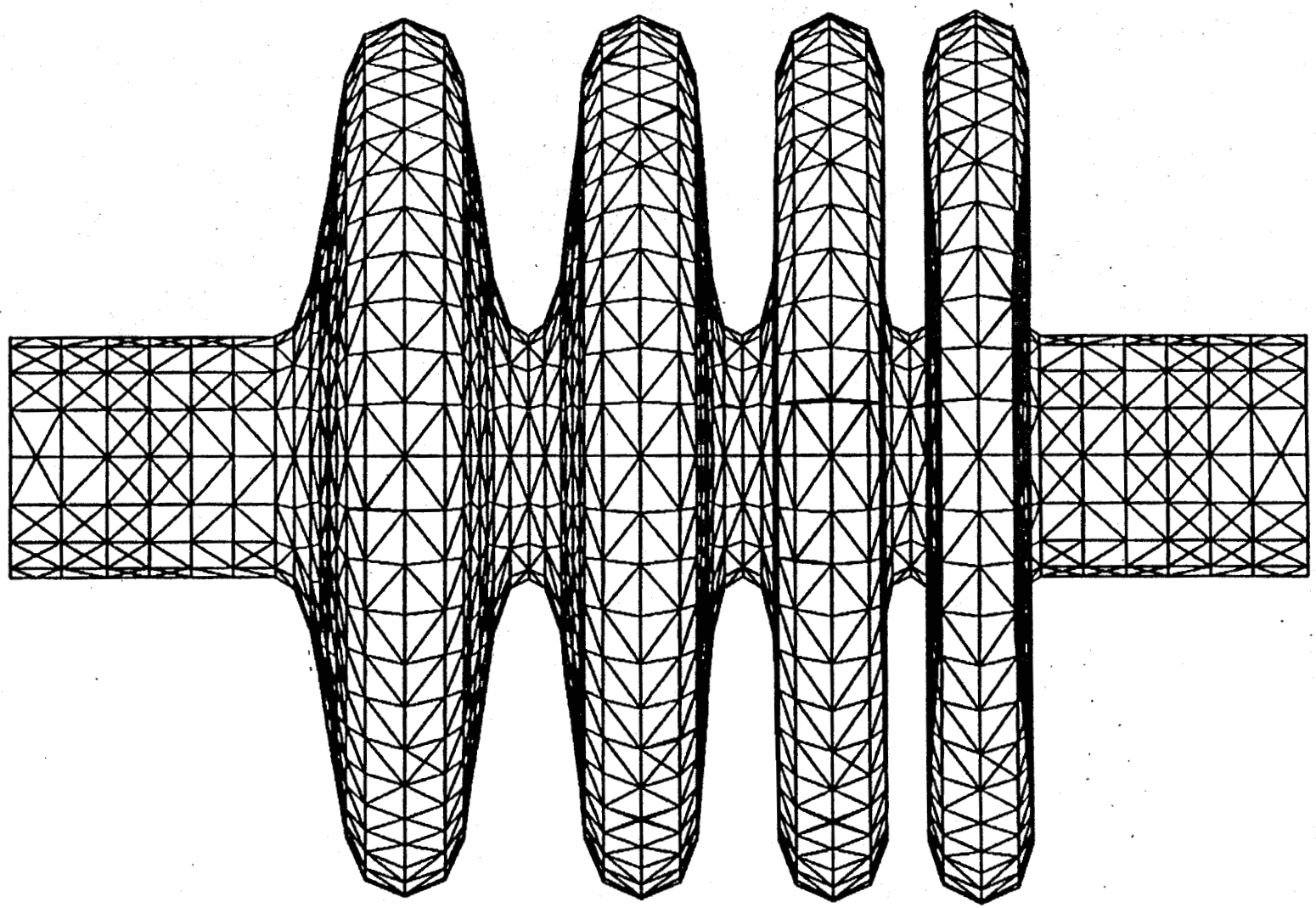

Figure VI-5: Finite Element Model of the First Axial Mode

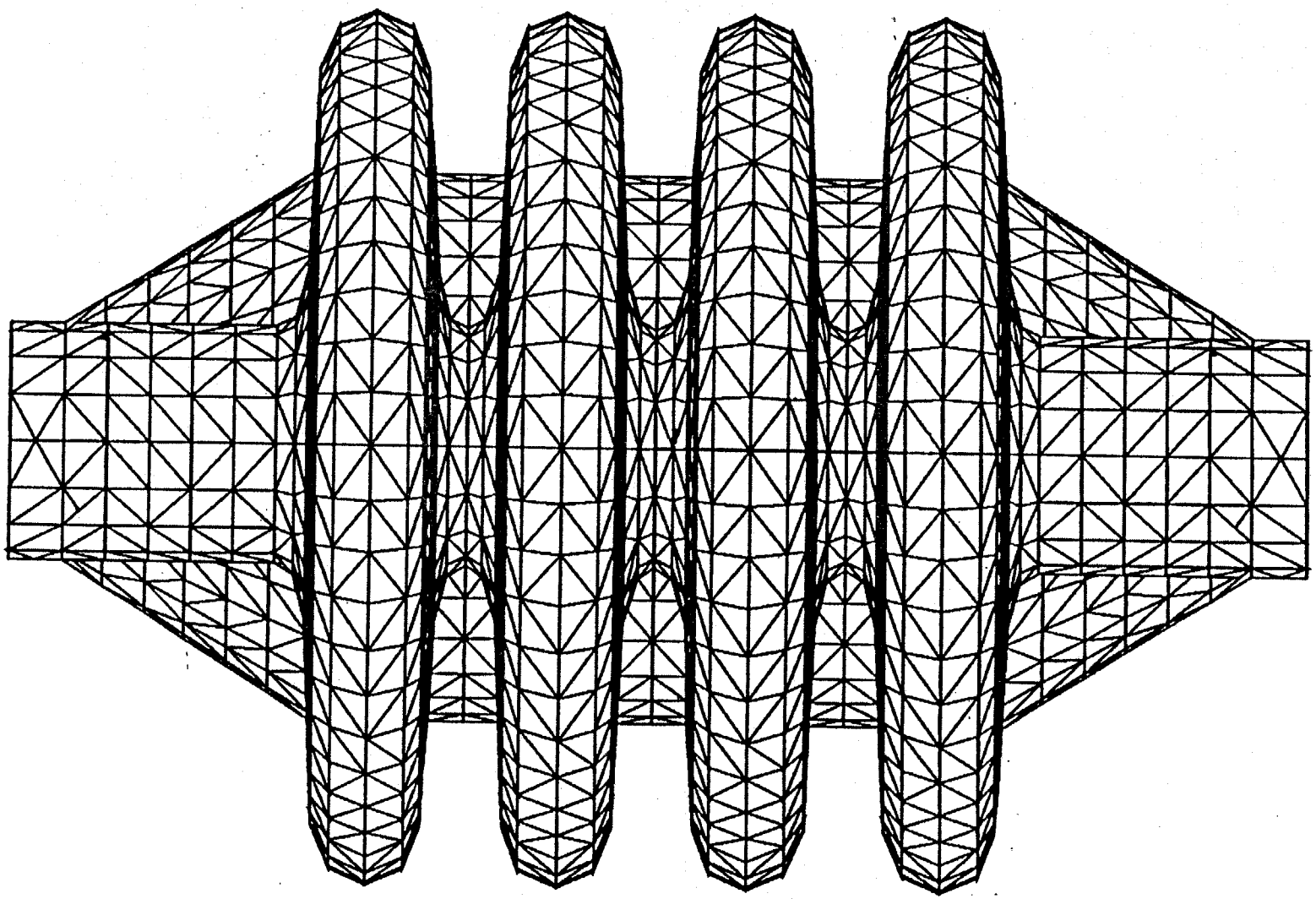

Figure VI-6: Cross-Section of the Radial and Cylindrical Stiffeners Used on the 4-Cell Cavity

Copies to:

R. Barber, ESA-DE, MS H821
J. Billen, AOT-1, MS H817
K. Bongardt, ESS
K. C. Chan, AOT-2, MS H838
Z. Chen, ESA-DE, MS H821
W. Clark, AOT-1, MS H817
W. Everett, AOT-1, MS H817
R. Garnett, AOT-1, MS H817
R. Gentzlinger, ESA-DE, MS H821
E. Gray, AOT-1, MS H817
A. Jason, AOT-1, MS H808
J. Kirkgessner, Cornell University
F. Krawczyk, AOT-1, MS H817
J. Lagniel, Saclay
G. Lawrence, LER-APT, MS H813
F. Martinez, AOT-1, MS H817
R. Martinez, AOT-1, MS H808
J. Mitchell, AOT-1, MS H808
A. Naranjo, AOT-1, MS H817
M. Pabst, ESS
H. Padamsee, Cornell University
H. Piel, University of Wuppertel
A. Rendon, AOT-1, MS H817
W. Rodriguez, ESA-DE, MS H821
P. Roybal, AOT-1, MS H817
B. Rusnak, AOT-1, MS H817
F. Sigler, AOT-1, MS H817
J. Stovall, AOT-DO, MS H817
H. Takeda, AOT-1, MS H817
T. Thompson, ESA-DE, MS H821
T. Wangler, AOT-1, MS H817
R. Wood, AOT-1, MS H817
L. Young, AOT-1, MS H817
AOT-DO, MS H850
AOT-1 Reading File, MS H817
ESA-DO, MS P945
CIC-10, MS A150
J. O'Toole, NGC.
J. Ratlke NGC
T. Sigu Itheiss, NGC